NOTE TO USERS

uOttawa

L'Université canadienne
Canada's university

FACULTÉ DES ÉTUDES SUPÉRIEURES ET POSTOCTORALES

uOttawa

L'Université canadienne
Canada's university

FACULTY OF GRADUATE AND POSDOCTORAL STUDIES

Zhichao Deng
AUTEUR DE LA THÈSE / AUTHOR OF THESIS

M.A.Sc. (Electrical Engineering)
GRADE / DEGREE

School of Information Technology and Engineering
FACULTÉ, ÉCOLE, DÉPARTEMENT / FACULTY, SCHOOL, DEPARTMENT

Mode Locked Fiber Lasers and their Application in Microwave Signal Generation
TITRE DE LA THÈSE / TITLE OF THESIS

J. Yao
DIRECTEUR (DIRECTRICE) DE LA THÈSE / THESIS SUPERVISOR

CO-DIRECTEUR (CO-DIRECTRICE) DE LA THÈSE / THESIS CO-SUPERVISOR

EXAMINATEURS (EXAMINATRICES) DE LA THÈSE / THESIS EXAMINERS

H. Anis

R. Gauthier

Gary W. Slater
LE DOYEN DE LA FACULTÉ DES ÉTUDES SUPÉRIEURES ET POSTDOCTORALES /
DEAN OF THE FACULTY OF GRADUATE AND POSTDOCORAL STUDIES

Mode Locked Fiber Lasers and their Application in Microwave Signal Generation

By

Zhichao Deng

Thesis submitted to the
Faculty of Graduate and Postdoctoral Studies
in partial fulfillment of the requirements for the degree of

Master of Applied Science
in
Electrical Engineering

Ottawa-Carleton Institute of Electrical and Computer Engineering

School of Information Technology and Engineering

Faculty of Engineering

University of Ottawa

May, 2005

Your file Votre référence
ISBN: 0-494-11253-0
Our file Notre référence
ISBN: 0-494-11253-0

ACKNOWLEDGEMENTS

I would like to express my deepest gratitude to my supervisor Dr. Jianping Yao for his knowledgeable guidance, helpful comments and suggestions, and constant encouragement during the period of my study.

I would also like to thank all the members of the Microwave Photonics Research Lab for their cooperation and friendship especially Jian Yao, Fei Zeng, Jun Wang, and Sébastien Blais for the valuable discussions with them. I have a good memory of the pleasant time working with them.

Finally, I give my greatest thanks to my parents for their endless love and support. I would like to dedicate this thesis to my wife Jie Qin, who always shares my challenges and achievements during my life. Without her love and support, I would never have finished my study.

I would like to thank all from the bottom of my heart!

ABSTRACT

An investigation of mode-locked fiber ring lasers and their applications in photonic generation of microwave signals is presented in this thesis. Both passive mode locking and active mode locking are investigated.

For the passive mode-locking, a fiber laser with figure-eight structure that incorporates a nonlinear amplifying loop mirror as a saturable absorber is proposed and demonstrated. One application of the demonstrated passively mode locked fiber ring laser is to generate high-quality microwave signals. In this thesis, a microwave signal generated by beating the mode-locked longitudinal modes at a photodetector is realized. The results show that the generated microwave signal has low phase noise with high stability.

Multiwavelength mode locked laser can find many applications in optical communications. In this thesis, a multiwavelength passively mode-locked fiber ring laser using cascaded fiber Bragg gratings is proposed and demonstrated. It is different from multiwavelength active mode locking in which the round-trip frequencies for all wavelengths must be identical; for passive mode locking, it is demonstrated theoretically and experimentally that the round-trip frequencies are not necessarily

identical. A three-wavelength fiber ring laser that is passively mode locked with non-identical round-trip frequencies is demonstrated.

Since the ring length of a fiber laser is usually very long, it leads to a small longitudinal mode spacing. The beating between the longitudinal modes will generate microwave signals at low frequency. Rational harmonic actively mode-locked fiber lasers can be used to generate microwave signals at much higher frequency. In this thesis, a rational harmonic actively mode-locked fiber laser is proposed and demonstrated. Stable rational harmonic active mode locking is realized and microwave signal generation by beating the mode-locked rational harmonics is demonstrated. To equalize the amplitude of the generated pulses or to suppress the lower-order harmonics, two techniques including the nonlinear polarization rotation technique and the nonlinear modulation technique are implemented. It is demonstrated that the technique using nonlinear modulation provides better lower-order harmonic suppression. A stable and low phase noise microwave signal with high lower-order harmonic suppression at 22 GHz is generated when the nonlinear modulation technique employed.

TABLE OF CONTENTS

LIST OF FIGURES

Chapter 1 Introduction

1.1 Background

Although the invention of the first fiber laser can be traced back to as early as 1961 by Snitzer using an Nd-doped fiber with a large core [Sni61], it did not draw much serious attention from researchers until the late 1980s, when the erbium-doped fiber amplifier (EDFA) was getting into practical use. It is this great invention that makes it possible to build up an all-fiber laser communication system, in which a fiber laser is used as a light source with the most important advantage of intrinsically low-loss coupling with other fiber-optic components. There are also other advantages of a fiber laser over its semiconductor counterpart, which include high output power, low noise, narrow linewidth, and wide wavelength tunable range.

However, two disadvantages have greatly limited the applications of fiber lasers in the area of optical communications. First, it is more difficult to develop a single longitudinal mode fiber laser than a single longitudinal mode semiconductor laser. This difficulty arises from the fact that the cavity length of a fiber laser is impossible to be as short as that of a semiconductor laser. This much longer cavity length of a

fiber laser leads to a much smaller longitudinal mode spacing: so small that there is hardly any optical filter that can be used to restrict the multiple longitudinal modes to one. Second, the performance of fiber lasers is greatly affected by environmental changes such as temperature, humidity and vibrations, because of the long cavity length. Great efforts have been directed to solve these problems. However, until today there are few applications of fiber lasers in optical communications systems.

Fiber lasers can also be used to generate ultra-short optical pulses (pico- or femto-second) at a repetition rate up to 200 GHz [Yos96]. Ultra-short optical pulses can find wide applications in high-speed communication systems. Ultra-short optical pulses are also promising candidates for exciting solitons inside optical fiber. Although soliton-based optical communication systems have not yet been implemented for real applications, it is so beautiful an idea that it has attracted a lot of interests. In addition, optical pulse trains generated by fiber lasers can also find many applications in other areas such as microwave photonics, fiber optic sensing, and optical signal processing.

The most widely used method to generate high-repetition rate and ultra-short optical pulse trains is to use mode-locked fiber lasers. As a matter of fact, it is the only method that has generated an optical pulse train with a repetition rate up to 10 GHz. Mode-locking is also a technique to produce ultra-short (as narrow as several femto-

seconds) and ultra-high power optical pulse trains. Because of the unique role of fiber lasers to generate high-repetition rate and ultra-short optical pulse trains, mode-locked fibers have been intensively investigated in the last few years.

In this thesis, we will investigate and demonstrate three types of mode-locked fiber ring lasers. Their applications in the generation of microwave signals will also be investigated.

1.2 Major contributions

1) A passively mode-locked fiber ring laser is implemented. A nonlinear amplifying loop mirror (NALM) with an EDFA is used as the mode-locker. With this NALM, a figure-eight laser (F8L) is built. Stable passive mode-locking is achieved. Beating signal with high spectrum quality is obtained by applying the output to a photodetector. The results show that passively mode-locked fiber ring lasers can be used to generate high-quality microwave signals.

2) A multiwavelength passively mode-locked fiber ring laser is demonstrated. Cascaded fiber Bragg gratings (FBGs) are incorporated into the F8L to get

multiwavelength output. It is different from active mode locking of a multiwavelength fiber laser in which the cavity length for all wavelengths must be identical. In a multiwavelength passively mode-locked fiber laser, mode locking can be easily established if the cavity lengths for different wavelengths are not identical.

3) A rational harmonic actively mode-locked fiber ring laser is investigated and demonstrated. A stable microwave signal with frequencies up to 22 GHz is generated by applying the laser output to a photodetector. Rational harmonic mode-locking is better than normal harmonic mode-locking since its repetition rate can be several times higher than the modulating frequency. Thus, it can generate optical pulses with higher repetition rate. One major limitation of rational harmonic mode locking is that the output pulses have severely uneven amplitudes. To reduce this nonuniformity, nonlinear polarization rotation technique and nonlinear modulation technique are utilized to equalize the amplitude in this thesis.

1.3 Thesis outline

This thesis consists of six chapters. In Chapter 1, a brief introduction to continuous-wave and mode-locked fiber lasers is presented, which serves as basis of the whole thesis. The major contributions of this research are also summarized in the chapter.

In Chapter 2, a detailed analysis of NALMs is presented. NALMs are widely used in pulsed fiber lasers to achieve passive mode-locking. In an NALM, the amplification is realized by using an EDFA. A brief discussion on EDFA is then provided in this chapter. An NALM is built. Simulation and experiments are carried out to study the performance of the NALM.

In Chapter 3, we investigate experimentally a single-wavelength passively mode-locked fiber laser for the generation of microwave signals. The laser has an F8L configuration. The condition to achieve soliton operation in the laser is discussed. The generation of microwave signals by applying the laser output to a photodetector is investigated. Microwave signals with frequencies equal to the integer numbers of mode spacing with good spectrum purity and high stability are obtained.

In Chapter 4, a multiwavelength passively mode-locked fiber laser is investigated. The difference between the single-wavelength and multiwavelength passively mode-locked fiber lasers in this thesis is that in the multiwavelength fiber laser, multiple

fiber Bragg gratings (FBGs) are cascaded in the laser cavity as the wavelength selecting element. Since the FBGs are located at different locations in the laser cavity, the round-trip frequencies for the wavelengths are different, active mode locking which requires an identical round-trip frequency is not possible. For passive mode locking, it is verified that the round-trip frequencies for different wavelengths are not required to be identical. In this chapter, a three-wavelength passively mode-locked fiber ring laser with non-identical round-trip frequencies is experimentally demonstrated.

To generate high-frequency microwave signals using mode-locked lasers, the repetition rate must be high. Rational harmonic active mode-locking is a technique to generate optical pulses with high repetition rate. In Chapter 5, rational harmonic active mode-locking is investigated. To equalize the pulse amplitude or to increase the lower-order harmonic suppression, two techniques including nonlinear polarization rotation technique and nonlinear modulation technique are investigated. A stable and low phase noise microwave signal with high lower-order harmonic suppression at 22 GHz is generated when the nonlinear modulation technique is employed.

At last, conclusions are drawn in Chapter 6. Some suggestions for further research are also presented in this chapter.

Chapter 2 Nonlinear amplifying loop mirror

Two techniques are used to achieve mode-locking: active mode locking and passive mode locking. In a passively mode locked fiber laser, the mode locking operation is usually realized by using a nonlinear device, serving as an optical switch. Nonlinear amplifying loop mirrors are widely used in fiber lasers to achieve passive mode locking. In this chapter, we will investigate theoretically and experimentally the nonlinear amplifying loop mirrors. Different passively mode-locked fiber lasers based on the nonlinear amplifying loop mirror will be investigated in chapters 3 and 4. Active mode locking of a fiber laser to generate high-repetition rate optical pulses will be investigated in chapter 5.

One basic way to achieve passive mode-locking is to incorporate a saturable absorber in the lasing cavity. The absorption of a saturable absorber is dependent on the intensity of the incident light. When the incident light is weak, its absorption is high so that the intensity of the transmitted light is low. When the incident light is strong, its absorption decreases dramatically so that the intensity of the transmitted light is very high. The curve of the intensity of the transmitted light versus that of the incident light is saturated after the input power reaches a certain value called threshold, this is where the name "saturable absorber" comes from. In this way, a

saturable absorber always clamps off the leading and trailing edges of the small spontaneous pulses, which may be caused by small noise, but transmits the peaks of those pulses with small loss. By repeating this process many times, the fiber laser will be finally passively mode locked. The final linewidth of the mode-locked laser is determined by the material property of the saturable absorber, the total dispersion, the nonlinearity, the loss, and the gain of the laser cavity.

Nonlinear optical loop mirror (NOLM) and nonlinear amplifying loop mirror (NALM) are two candidates serving as the saturable absorber in a passively mode locked fiber laser.

2.1 Nonlinear optical loop mirror

An NOLM can be used as an optical saturable absorber if a segment of the fiber within the loop has a high nonlinearity. Since an NOLM is a special type of fiber loop mirror, it is helpful to start the discussion from normal fiber loop mirror.

2.1.1 Fiber loop mirror

A fiber loop mirror can be constructed by splicing a length of fiber from the two output ports of a 4-port fused fiber coupler with a power splitting ration of α : (1−α), as shown in Fig. 2-1 [Mor88]. If the input electric filed at port 1 is E_I, based on coupled mode theory [Oka00], the output electric fields at port 3 and port 4 should be $E_{I3} = \sqrt{\alpha} e^{-j\beta z} E_I$ and $E_{I4} = -j\sqrt{1-\alpha} e^{-j\beta z} E_I$, respectively. It is easily seen that there is a phase difference of $\frac{\pi}{2}$ between the electric fields at the two output ports.

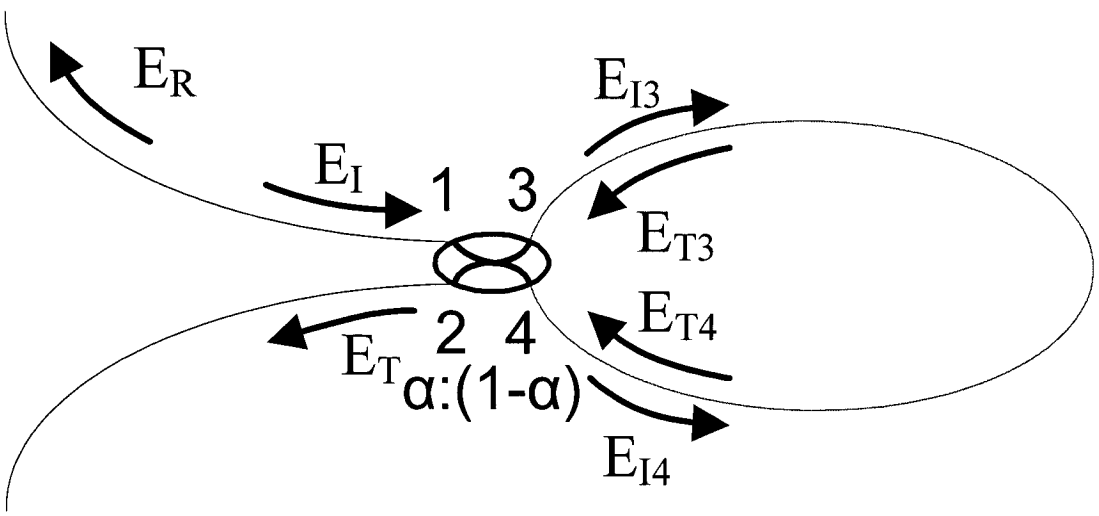

Fig. 2-1. Fiber loop mirror.

Let us denote the power of the incident light at port 1 of the coupler as P_I. The power splitting ratio of the coupler is $\alpha:(1-\alpha)$, therefore the power of the output lights at

port 3 and port 4 are αP_I and $(1-\alpha)P_I$. According to the coupled mode equation, the electrical fields of the output lights are

$$E_{I3} = \sqrt{\alpha} e^{-j\beta z} E_I, \tag{2-1}$$

$$E_{I4} = -j\sqrt{1-\alpha} e^{-j\beta z} E_I, \tag{2-2}$$

where β is the propagation constant of the fiber, βz is the phase delay introduced by the coupler.

The output lights E_{I3} and E_{I4} are then transmitted in two different directions inside the fiber loop. When they return to the coupler, their electric fields can be expressed by

$$E_{T4} = e^{-j\beta L} E_{I3} = \sqrt{\alpha} e^{-j\beta z} e^{-j\beta L} E_I, \tag{2-3}$$

$$E_{T3} = e^{-j\beta L} E_{I4} = -j\sqrt{1-\alpha} e^{-j\beta z} e^{-j\beta L} E_I, \tag{2-4}$$

where L is the length of the fiber loop.

These two light waves are then split by the coupler again to port 1 and port 2, and they will interfere at the two ports. Again using the coupled mode equation, the light coupled from E_{T4} to port 2 is

$$E_{T4-2} = \sqrt{\alpha} e^{-j\beta z} E_{T4} = \alpha e^{-j2\beta z} e^{-j\beta L} E_I, \tag{2-5}$$

$$E_{T3-2} = -j\sqrt{1-\alpha} e^{-j\beta z} E_{T3} = -(1-\alpha) e^{-j2\beta z} e^{-j\beta L} E_I. \tag{2-6}$$

Therefore, the finally transmitted light from port 2 is

$$E_T = E_{T4-2} + E_{T3-2} = (2\alpha - 1) e^{-j2\beta z} e^{-j\beta L} E_I. \tag{2-7}$$

Based on the similar process, we can get the reflected light from port 1

$$E_R = -j2\sqrt{\alpha(1-\alpha)} e^{-j2\beta z} e^{-j\beta L} E_I. \tag{2-8}$$

Based on Equations (2-7) and (2-8), we can easily get the transmission and reflectivity of the fiber loop:

$$T = \frac{P_T}{P_I} = \frac{|E_T|^2}{|E_I|^2} = \frac{(2\alpha-1)^2 |E_I|^2}{|E_I|^2} = (2\alpha - 1)^2, \tag{2-9}$$

$$R = \frac{P_R}{P_I} = \frac{|E_R|^2}{|E_I|^2} = \frac{4\alpha(1-\alpha)|E_I|^2}{|E_I|^2} = 4\alpha(1-\alpha). \tag{2-10}$$

From Equations (2-9) and (2-10), it is clearly seen that the power transmission and reflectivity of a fiber loop mirror are dependent on the power splitting ratio of the coupler used in the fiber loop. Fig. 2-2 shows this dependence. The transmission will reduce from 1 to 0 while the power splitting ratio increases from 0 to 0.5. Therefore, for a fiber loop employing a 3-dB coupler (0.5 power splitting ratio), there is no any

transmitted light, and all the input light will be reflected back, just like a mirror with 100% reflection. This is how the name fiber loop mirror comes.

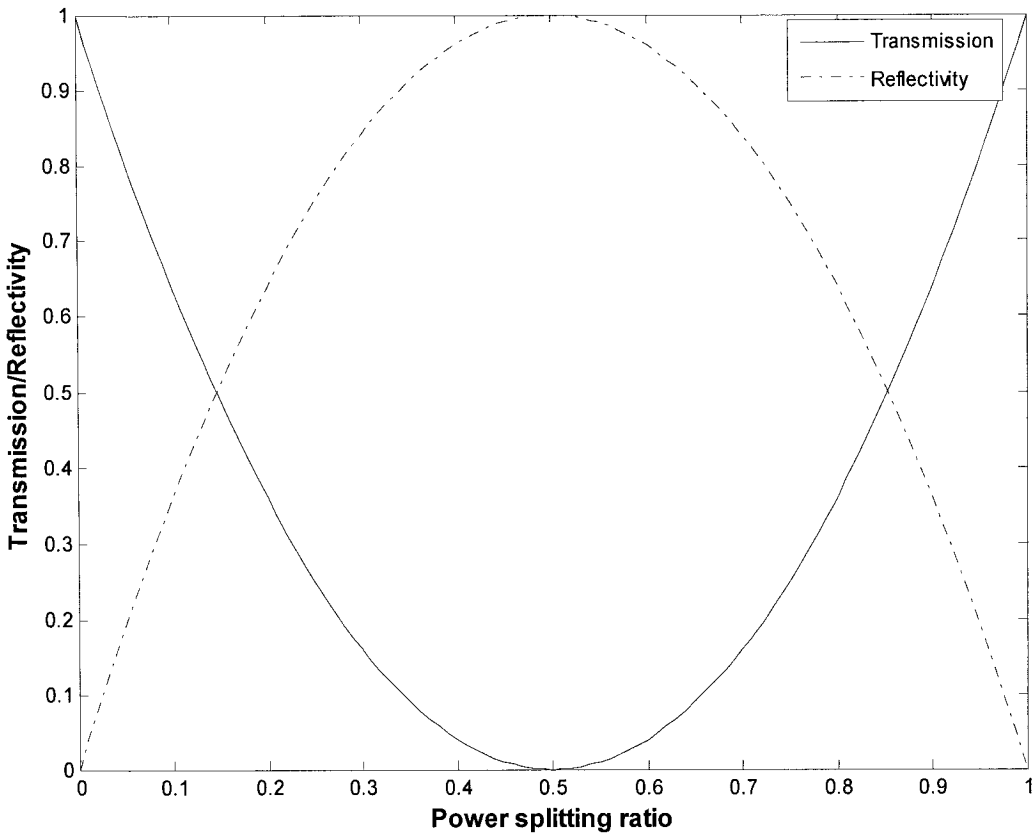

Fig. 2-2. Simulated transmission and reflectivity of a fiber loop mirror for different power splitting ratio.

2.1.2 Nonlinear effect in the fiber loop mirror

In the above discussion, the refractive index of the silica fiber is assumed to be independent of the power of the light propagating inside that fiber. In reality, however, the silica fiber will behave as a nonlinearly device when the power of light is high enough: its refractive index will increase when the intensity of the light is higher. The refractive index change can be expressed as [Agr01]

$$n = n_0 + n_2 \frac{P}{A_{eff}} = n_0 + n_2 I \,, \tag{2-11}$$

where n is the refractive index, n_0 is the original refractive index, n_2 is the nonlinear-index coefficient, P is the optical power, A_{eff} is the effective mode field area, and I is the intensity of the light inside the fiber core. The typical value of n_2 for silica fiber is about $2.6\times10^{-20} m^2/W$. It varies if the fiber core is doped with other materials.

The propagation constant β is no longer a constant, but a function of the light intensity in the fiber core

$$\beta = \frac{2\pi}{\lambda} n = \beta_0 + \frac{2\pi}{\lambda} n_2 I \,, \tag{2-12}$$

where λ is the wavelength of the light wave in vacuum, and β_0 is the original propagation constant.

By taking into account the nonlinear effect inside the fiber loop, some interesting properties can be found [Dor88]. Because of the existing of nonlinearity in the loop mirror, it is called nonlinear optical loop mirror (NOLM).

In the following, we will present a brief analysis on the NOLM. Using the same process as for the fiber loop mirror, we have

$$E_{T4} = e^{-j\beta L} E_{I3} = \sqrt{\alpha} e^{-j\beta_0 z} e^{-j\beta_0 L} e^{-j2\pi n_2 \alpha I_I L/\lambda} E_I , \tag{2-13}$$

$$E_{T3} = e^{-j\beta L} E_{I4} = -j\sqrt{1-\alpha} e^{-j\beta_0 z} e^{-j\beta_0 L} e^{-j2\pi n_2 (1-\alpha) I_I L/\lambda} E_I . \tag{2-14}$$

Since the nonlinear effect inside the fiber loop is taken into account, a nonlinear term depending on n_2, αI_I or $(1-\alpha)I_I$, L, and λ is therefore added.

Then the transmitted light from port 2 can be obtained

$$\begin{aligned} E_T &= E_{T4-2} + E_{T3-2} \\ &= e^{-j2\beta_0 z} e^{-j\beta_0 L} E_I \left[\alpha e^{-j2\pi n_2 \alpha I_I L/\lambda} - (1-\alpha) e^{-j2\pi n_2 (1-\alpha) I_I L/\lambda} \right]. \end{aligned} \tag{2-15}$$

Also the reflected light from port 1 is

$$E_R = -j\sqrt{\alpha(1-\alpha)} e^{-j2\beta_0 z} e^{-j\beta_0 L} E_I \left[e^{-j2\pi n_2 \alpha I_I L/\lambda} + e^{-j2\pi n_2 (1-\alpha) I_I L/\lambda} \right]. \tag{2-16}$$

By introducing the term ϕ_{NL} for the phase delay induced by the nonlinear effect

$$\phi_{NL} = \frac{2\pi n_2 (1-2\alpha) I_I L}{\lambda}, \tag{2-17}$$

the intensities of the transmitted and reflected light waves can be expressed as

$$|E_T|^2 = |E_I|^2 [1 - 2\alpha(1-\alpha)(1+\cos\phi_{NL})], \tag{2-18}$$

$$|E_R|^2 = |E_I|^2 2\alpha(1-\alpha)(1+\cos\phi_{NL}). \tag{2-19}$$

Therefore, we finally get the power transmission and reflectivity of an NOLM

$$T = \frac{P_T}{P_I} = \frac{|E_T|^2}{|E_I|^2} = 1 - 2\alpha(1-\alpha)(1+\cos\phi_{NL}), \tag{2-20}$$

$$R = \frac{P_R}{P_I} = \frac{|E_R|^2}{|E_I|^2} = 2\alpha(1-\alpha)(1+\cos\phi_{NL}). \tag{2-21}$$

Fig. 2-3 shows the simulated power transmission of an NOLM as a function of $I_I L$. Three different power splitting ratios 0.1, 0.2, and 0.4 are considered. Other parameters used in the simulation are $n_2 = 2.6\times10^{-20} m^2/W$, $\lambda = 1550nm$. From Fig. 2-3 it is clearly seen that the transmissions are periodic. According to Equations (2-17) and (2-20), the period of $I_I L$ is $\frac{\lambda}{n_2(1-2\alpha)}$. Therefore, the first peak is found when $I_I L$ equals to half of this period, that is

$$I_I L = \frac{\lambda}{2n_2(1-2\alpha)}. \tag{2-22}$$

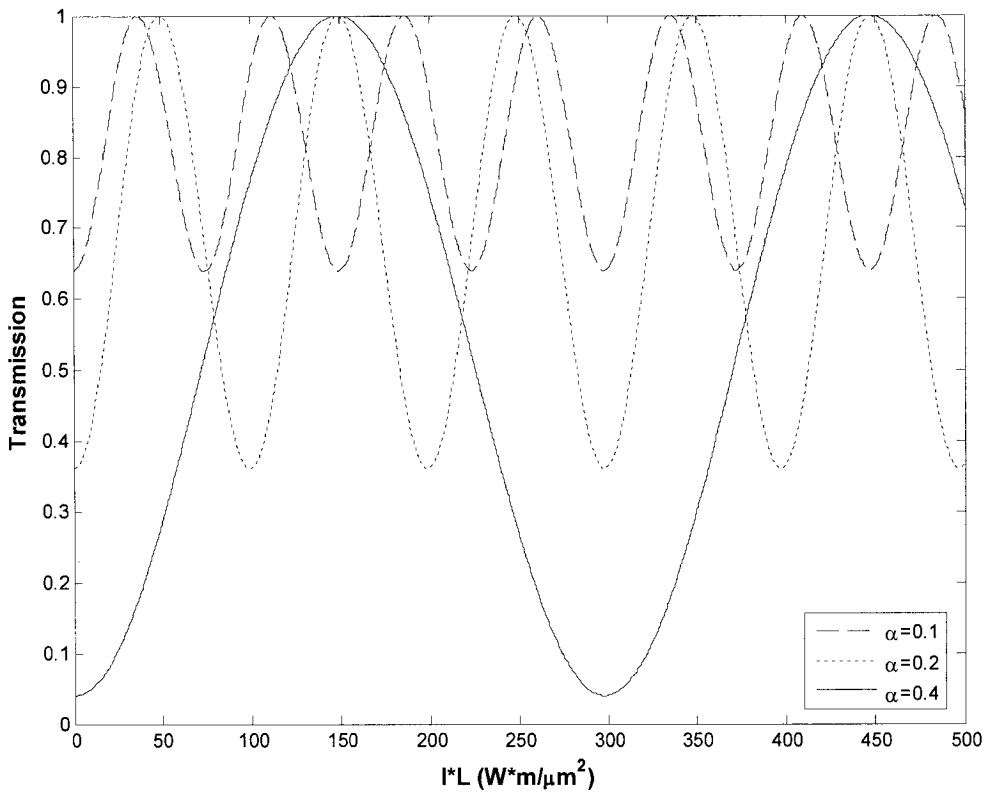

Fig. 2-3. Transmission of an NOLM as a function of $I_I L$ for different power splitting ratios.

The transmission in Fig. 2-3 suggests that an NOLM can be used to perform optical switching [Fer90]. For a fixed optical intensity, to reduce the loop length, we may use an optical coupler with a smaller power splitting ratio. As can be seen from Fig. 2-3,

the period is reduced when the splitting ratio is smaller. But this is not preferred since smaller α will result in a smaller extinction ratio. Another method to reduce the fiber length is to increase the input light intensity I_I, which can be achieved by reducing the effective area A_{eff} of fiber core. It is known that dispersion shifted fibers (DSFs) have smaller effective core areas and therefore can be used to construct an NOLM. Fig. 2-4 shows an NOLM using a length of DSF.

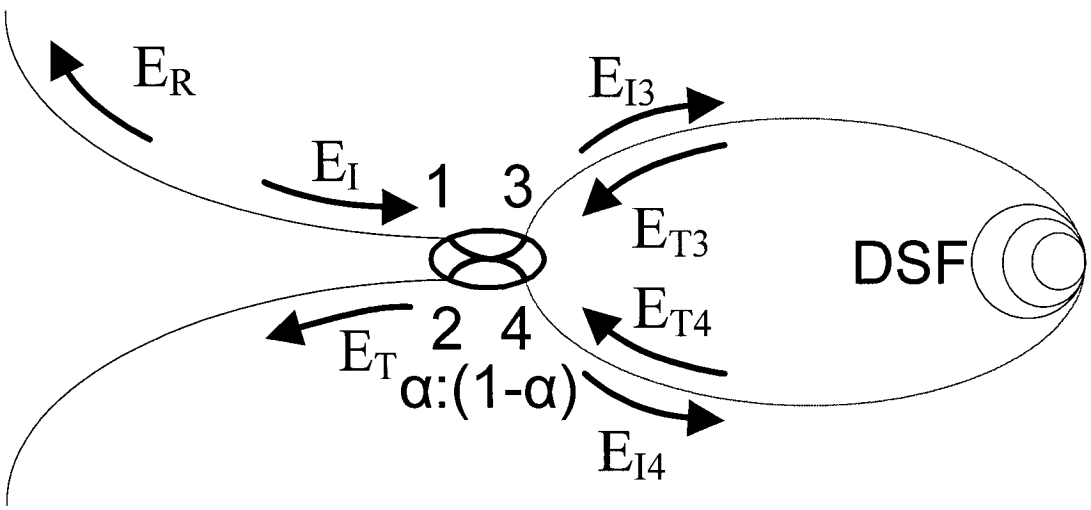

Fig. 2-4. Nonlinear optical loop mirror utilizing the dispersion shifted fiber.

As discussed earlier, the period of the transmission function is dependent on the power splitting ratio of the optical coupler. For an optical coupler with a power splitting ratio approaching 0.5, the period of the transmission function would

approach infinity based on Equation (2-22). Therefore, an optical coupler with 0.5 power splitting ratio (or 3-dB coupler) cannot be used in an NOLM. The reason to this is that an NOLM must maintain certain nonreciprocal unbalance for the nonlinear loop to switch the input light from one port to another. An unbalanced coupler generates counter-propagating lights with different intensity inside the nonlinear loop, and these two light waves cumulate different nonlinear phase shifts when they travel back to the coupler and then interfere with each other. It is the phase difference between these two light waves that would result in the switching of light from the input port to the output port. Therefore, to keep the nonreciprocal unbalance is important for the operation of an NOLM.

2.2 Nonlinear amplifying loop mirror

NOLMs have been widely used in many fiber-optic systems for applications such as passive mode locking [Bul90], optical thresholding [Sot02], and optical switching [Moo91]. There are, however, some disadvantages that limit the applications of NOLMs. One major disadvantage is that the extinction ratio is dependent on the power splitting ratio. To have a higher extinction ratio, the power splitting ratio should be closer to 0.5. On the other hand, the period of the transmission function approaches infinity when the power splitting ratio approaches 0.5, as can be seen

from Fig. 2-3. A larger period means a higher light intensity in the fiber core to achieve the light switching.

To maintain a small period, an improved nonlinear fiber loop mirror, called nonlinear amplifying loop mirror (NALM), was proposed [Fer90]. In an NALM, a 3-dB coupler can be used to obtain the largest extinction ratio. The nonreciprocal unbalance inside the nonlinear loop is maintained if the amplifier is located at a point that is closer to one end of the 3-dB coupler. Therefore, the intensities of the two counter-propagating light waves are different when they reach the DSF, which leads to different nonlinear phase shifts for the two light waves.

In most cases, the amplifier used in an NALM is an EDFA. In the following, a brief discussion on EDFAs is presented.

2.2.1 Erbium-doped fiber amplifier

The first EDFA was invented in 1987 by Mears et al. [Mea87]. This invention has revolutionized the whole fiber-optics field. One area that benefits greatly from this invention is the dense wavelength division multiplexing (DWDM) for long-haul optical communications. The application of EDFAs has made it possible to multiplex

tens even hundreds of wavelength channels over a single fiber without significantly increasing the complexity and cost of the communications systems. The development of EDFAs has also stimulated research activities in other areas such as fiber lasers, fiber-optic sensors and fiber-optic instrumentation.

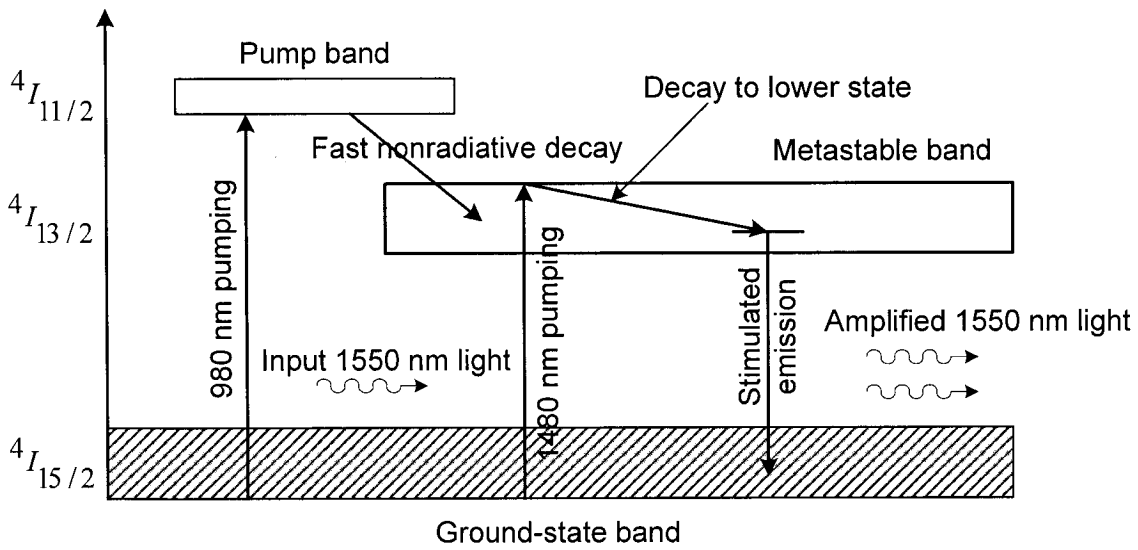

Fig. 2-5. Energy-level diagram of erbium ions in silica fiber.

In an EDFA, a length of erbium-doped fiber (EDF) pumped by a light source is used to provide the gain. Fig. 2-5 shows the simplified energy-level diagram of erbium ions in silica glass. Two energy levels corresponding to two wavelengths of 980 nm and 1480 nm are shown in the diagram. To promote electrons at ground-state band to the pump band, pumping source emitting at 980 nm or 1480 nm should be used. The

electrons promoted to the pump band will decay quickly to the meta-stable band, and the population inversion is then established. If an input light, which should be in the wavelength range of 1530-1560 nm, is injected into the EDF, stimulated emission will take place, and the input light is then amplified.

The advantages of EDFAs over semiconductor optical amplifiers (SOAs) include intrinsic low coupling loss with other fiber-optic devices, large gain (typically 30-40 dB), and low noise figure. These features make EDFAs very suitable for fiber-optic systems. However, EDFAs also have some disadvantages. One of those is that the saturation point is not high enough. This means that once the output power of the EDFA exceeds its saturation point (usually only several dBm), the gain of the EDFA will decrease very sharply. For most of the applications, this is not a big problem: the system can be working in the saturated region. But for the application in an NALM, this may causes problems. This point is discussed in detail in Section 2.3.

2.2.2 Nonlinear amplifying loop mirror with the erbium-doped fiber amplifier

NALM was first proposed in 1990 [Fer90]. In addition to its intensive applications in passively mode-locked fiber lasers, in which it is used as a saturable absorber [Ric91a], an NALM can also be used as an optical switch with a low switching

threshold [Fer90]. All these applications are based on the nonlinear property of an NALM in which the power transmission has a nonlinear relationship with the input light intensity. For low intensity input, the output is highly attenuated. When the input light intensity is increased to reach a threshold, the NALM will have a significantly increased transmission.

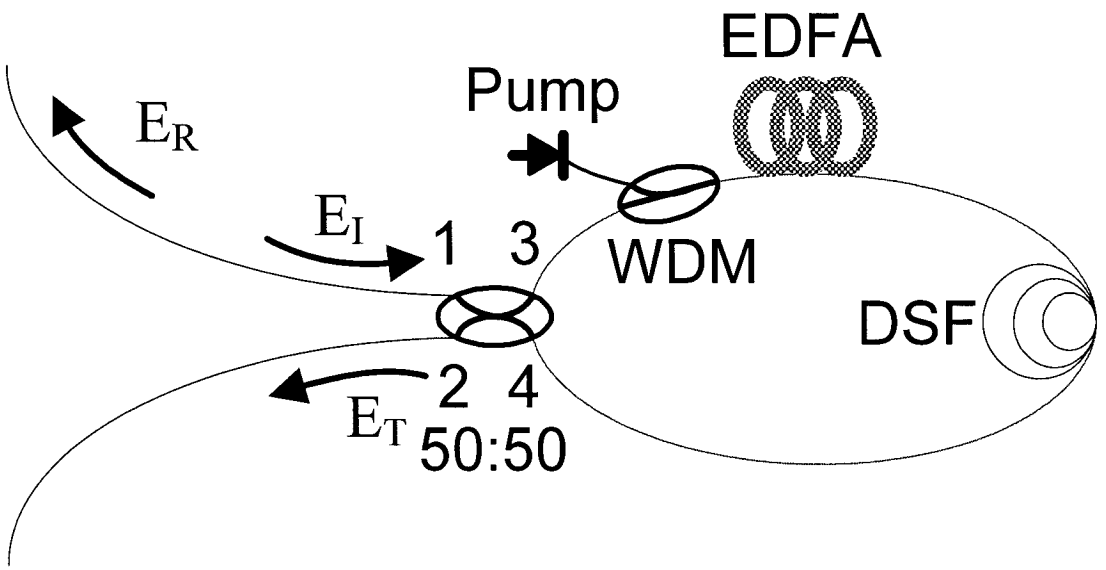

Fig. 2-6. Nonlinear amplifying loop mirror utilizing the erbium-doped fiber amplifier.

Fig. 2-6 shows the structure of an NALM with an EDFA. Here the input light E_I is divided equally by the 3-dB coupler into E_{I3} and E_{I4}. E_{I3} is amplified by the EDFA before it reaches the DSF, while E_{I4} reaches the DSF first and is amplified

afterwards. Therefore, although the intensities of the two light waves are identical while leaving the 3-dB coupler, when they travel back to the coupler, they experience different phase shifts. Thus we get the electric fields of the two light waves when they return to the coupler

$$E_{T4} = E_{I3}\sqrt{G}e^{-j\beta L} = \frac{\sqrt{2}}{2}\sqrt{G}e^{-j\beta_0 z}e^{-j\beta_0 L}e^{-j2\pi n_2 G I_I L/(2\lambda)}E_I, \tag{2-23}$$

$$E_{T3} = E_{I4}e^{-j\beta L}\sqrt{G} = -j\frac{\sqrt{2}}{2}\sqrt{G}e^{-j\beta_0 z}e^{-j\beta_0 L}e^{-j2\pi n_2 I_I L/(2\lambda)}E_I, \tag{2-24}$$

where G is the power gain of the EDFA.

Then the transmitted light wave can be written as

$$\begin{aligned} E_T &= E_{T4-2} + E_{T3-2} = \frac{\sqrt{2}}{2}e^{-j\beta_0 z}E_{T4} + \left(-j\frac{\sqrt{2}}{2}\right)e^{-j\beta_0 z}E_{T3} \\ &= e^{-j2\beta_0 z}e^{-j\beta_0 L}\frac{\sqrt{G}}{2}E_I\left[e^{-j2\pi n_2 G I_I L/2\lambda} - e^{-j2\pi n_2 I_I L/(2\lambda)}\right] \end{aligned}. \tag{2-25}$$

From Equation (2-25), we get the power of the transmitted light

$$\begin{aligned} P_T &= P_I\frac{G}{4}\left\{1+1-2\cos\left[-\frac{2\pi n_2 G I_I L}{2\lambda} + \frac{2\pi n_2 I_I L}{2\lambda}\right]\right\} \\ &= P_I G\sin^2\left(\frac{G-1}{4}kn_2 I_I L\right) \end{aligned}, \tag{2-26}$$

where P_I is the input light power, and $k = \frac{2\pi}{\lambda}$ is the propagation constant in vacuum.

The equation can be further simplified in the case of small signal:

$$P_T \approx P_I \frac{G(G-1)^2}{16}(kn_2 L I_I)^2 = P_I^3 \frac{G(G-1)^2}{16}\left(\frac{kn_2 L}{A_{eff}}\right)^2. \qquad (2\text{-}27)$$

The reflected light power can be calculated based on the energy conservation:

$$P_R = GP_I - P_T. \qquad (2\text{-}28)$$

Fig. 2-7 shows the simulation results of the transmitted and reflected light powers of an NALM. In the simulation, $\lambda = 1550nm$, $n_2 = 2.6\times10^{-20} m^2/W$, $A_{eff} = 30\mu m^2$, *L=200 m*, and *G=45 dB*. From this figure, it can be seen that the power of the transmitted light will be increasing when the input light power increases. But after the input light power increases to reach a threshold, the transmitted light power will be decreasing. The overall output light power then will be switched over from the transmitted port to the reflected port. The switching over will continue when the input light power keeps increasing. From Equation (2-26), it is easy to get the threshold of the input light power for the switching over

$$P_{I-th} = \frac{\lambda A_{eff}}{n_2 L(G-1)}. \qquad (2\text{-}29)$$

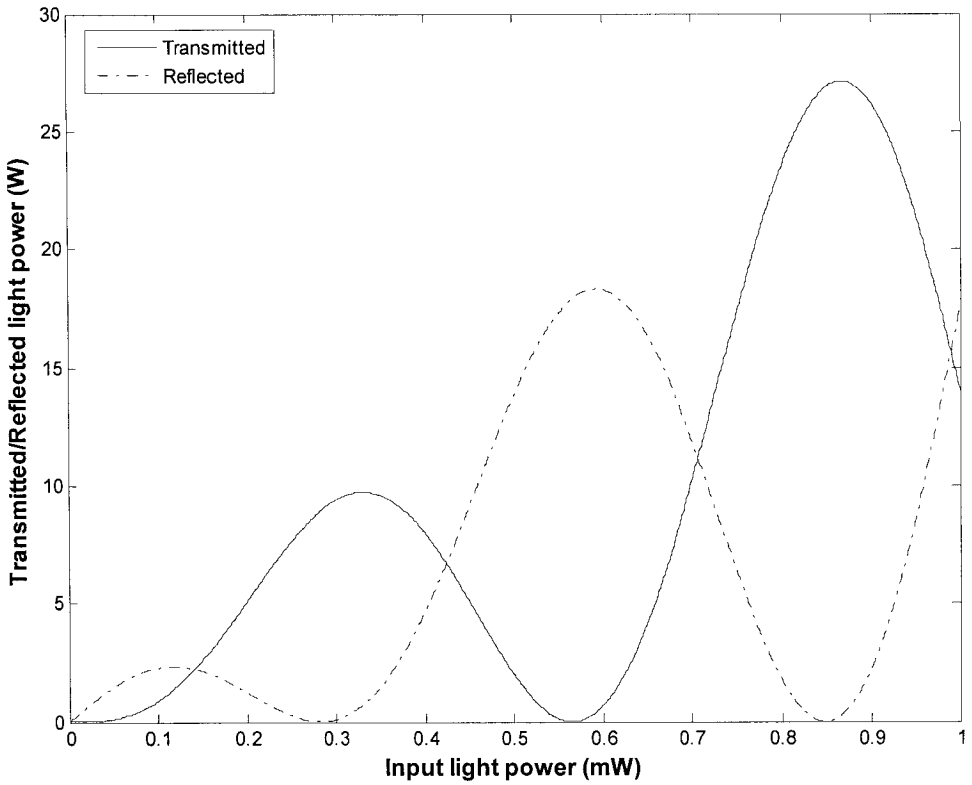

Fig. 2-7. Transmitted and reflected light power versus input light power of an NALM.

2.3 Characterization of a nonlinear amplifying loop mirror

Although the nonlinearity of an NALM is very clear in theory, it is difficult to measure the nonlinearity characteristics directly. There are two reasons. Firstly, the gain of the EDFA inside the fiber loop will decrease dramatically when the EDFA is saturated. To measure the characteristics of an NALM precisely, the gain of the

EDFA should be maintained the same during the measurement. Therefore, the input light power must be restricted to be very low, usually less than several milli-watts, to avoid the saturation of the EDFA. Second, one can clearly see from Fig. 2-7 that in order to observe the switching over of the output light power from the transmitted port to the reflected port, the input light power should be as large as several hundred micro-watts. The difficulty in choosing an appropriate input light power is the reason why few people demonstrated the relationship between input and transmitted light in small input signal region.

To overcome this difficulty, a special technique was proposed by Richardson et al. In their paper [Ric90], they suggested that the input light could be modulated by a square wave with a very small duty cycle. In this way, the average power of the input light will be very small while the peak power can be very large. Because the saturation point of the EDFA is dependent on the average input power over a couple of milli-seconds [Dut98], the EDFA can still be working in its linear region. On the other hand, as the nonlinear phase delay can be established in several femto-seconds [Tri88], the very high peak power of the input light can be strong enough to switch over the output light from the transmitted port to the reflected port.

Based on this technique, an experiment is carried out to measure the characteristics of an NALM. The experimental set up is shown in Fig. 2-8. The light output from a

1550-nm laser diode (LD) is applied to an intensity modulator, to which a square-wave pulse train generated by a pulse generator is applied. The pulse train has a pulse width of 20 ns and a repetition rate of 500 Hz with rising and falling time of 5 ns. Since the duty cycle of the pulse train is as low as 1×10^{-6}, the average power of the input light is much lower than the peak power of the input light. Hence, this modulated input light can keep the EDFA working in its linear region, at the same time cause the switching over of the NALM. The transmitted light is sent to a photodiode and the output pulse train is then monitored by a sampling oscilloscope.

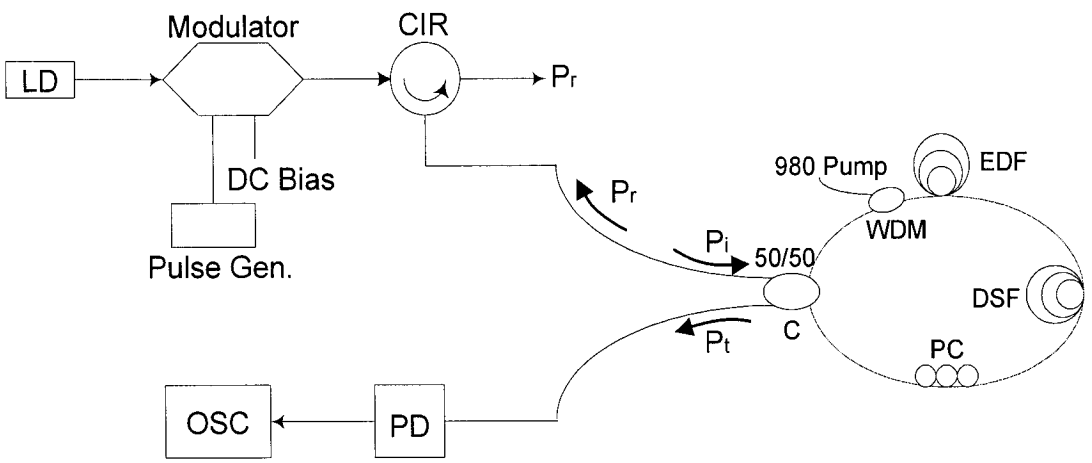

Fig. 2-8. Experimental setup for measuring the characterization of an NALM.

The measurement is carried out for two different situations: the input light has a low or high power. When the power of input light P_I is very low, Equation (2-27) shows

that the power of the transmitted light should be proportional to the third order of the power of the input light.

When the input light power is increased to reach the threshold, the transmitted light power will begin to decrease, and the output light will be switched over from the transmitted port to the reflected port, as can be seen from Fig. 2-7.

The experimental result for the situation of large input light power is shown in Fig. 2-9. In this situation, the power of the 980-nm pump laser is set at its maximum, in order to have a high gain of the EDFA. As indicated by Equation (2-29), a high EDFA gain will lead to a reduced threshold of the input light power to achieve the switching over. In this case, the gain of the EDFA is measured to be about 43 dB.

As can be seen from Fig. 2-9, the transmitted light power reaches its first maximum when the input light power is increased to 700 μW. When the input power is further increased, the transmitted power is decreased until a minimum is obtained when the input light power is at around 1250 μW. The experimental values agree quite well with the calculations. A small discrepancy near the minimum value of transmitted light power is observed, which is mainly attributed to the inaccuracy of the coupler power splitting ratio.

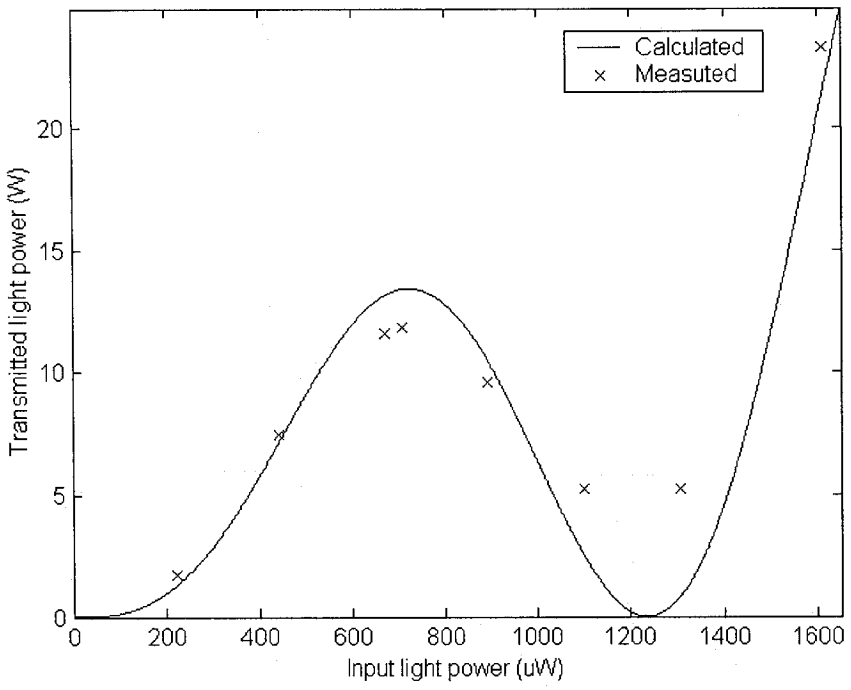

Fig. 2-9. Input light power versus transmitted light power for large input signal.

Fig. 2-10 shows the property of the NALM as a saturable absorber. As stated above, this measurement must be done in the small input signal region. To ensure the noise level of the EDFA is with the input signal, the power of the 980-nm pump laser is reduced to a quarter of its maximum. As a result, the gain of the EDFA is reduced to about 37 dB, which causes the curve of the transmitted light power versus the input light power to be less steep. However, according to the measured results, it is still clearly shown that the transmitted light power increases faster than the input light power does. This result reveals that an NALM can be used to achieve passive mode locking.

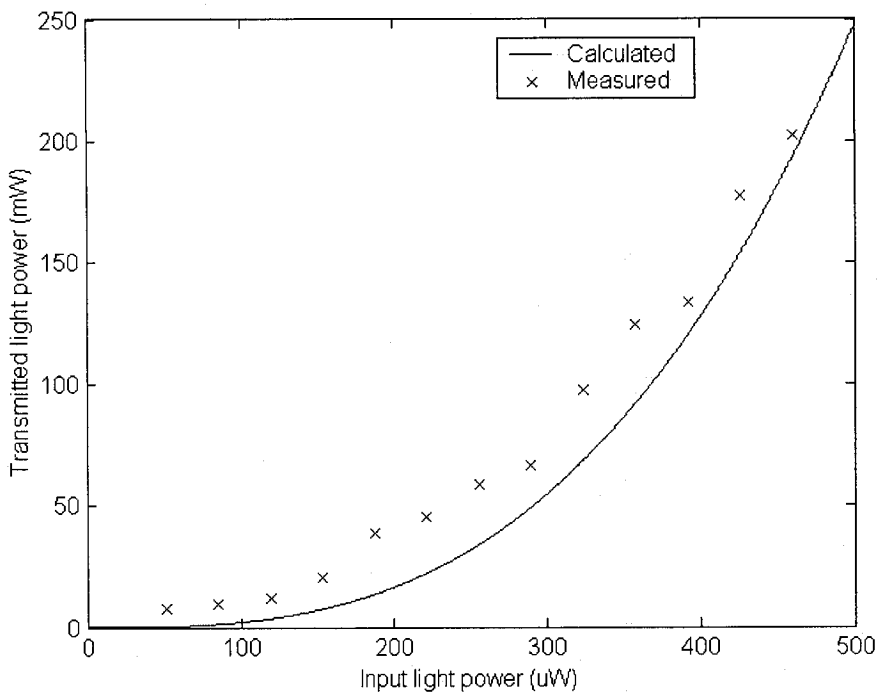

Fig. 2-10. Input light power versus transmitted light power for small input signal.

2.4 Summary

In this Chapter, a discussion on the fiber loop mirror, NOLM, and NALM was presented. Detailed analysis and simulations for these three types of fiber loop mirror were given. The applications of NOLMs and NALMs to passive mode locking and optical switching were introduced.

To investigate experimentally the nonlinearity of an NSLM, a special method was used to measure the characteristics of the NALM. To ensure that the EDFA in the NALM was not saturated in all circumstances, the input light wave was modulated by a square-wave signal with very low duty cycle. The average power of the optical signal was low, which ensured that the EDFA was always operating in the linear region. In addition, measurements in two situations with large and small input signals were carried out. The experimental results agreed well with the theoretical values.

Chapter 3 Single wavelength passively mode-locked fiber ring laser

Utilizing the NALM as a saturable absorber, a special kind of fiber laser, figure-eight laser, can be constructed to generate passively mode-locked optical pulses. This passively mode-locked laser, as well as its application in photonic generation of microwave signal will investigated is this chapter. As the optical pulses in figure-eight laser will evolve into optical solitons, a brief discussion to the property of soliton will also be included in this chapter.

3.1 Passive mode locking

In Chapter 2, a brief discussion was presented to explain why a saturable absorber can help to build up passive mode locking. In this chapter, a more detailed discussion will be presented.

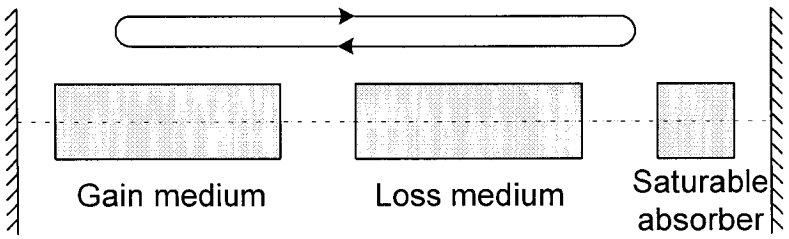

Fig. 3-1. Diagram of a passively mode-locked laser incorporating a saturable absorber.

In fact, for passive mode-locking using a saturable absorber, the laser cavity can be considered to have three separated sections [Hau75]: the gain medium, the loss medium, and the saturable absorber.

The steady-state electric filed in the laser cavity can be expressed by

$$\hat{T}_g \hat{T}_l \hat{T}_{sa} A(t) = A(t), \tag{3-1}$$

where $A(t)$ is the amplitude of the electric filed at any given position within the laser cavity, $\hat{T}_g$, $\hat{T}_l$, and $\hat{T}_{sa}$ are the operators for the round-trip evolution of electric filed of the gain medium, the loss medium, and the saturable absorber, which are respectively given by [Hau75]

$$\hat{T}_g = \left\{ 1 + g_0' \left[1 + \left(\frac{2}{\Delta\omega_0} \right)^2 \frac{d^2}{dt^2} \right] \right\}, \tag{3-2}$$

$$\hat{T}_l = 1 - \gamma_c, \tag{3-3}$$

$$\hat{T}_{sa} = 1 - \gamma' + \gamma' \frac{|A|^2}{I_s}, \tag{3-4}$$

where g_0' is the saturated gain, $\Delta\omega_0$ is the full width at half maximum (FWHM) of the laser line, γ_c is the cavity loss without the saturable absorber, γ' is the unsaturated loss of the saturable absorber, and I_s is the saturation intensity of the saturable absorber.

Substituting Equations (3-2), (3-3), and (3-4) into Equation (3-1), and assuming that $(g_0', \gamma_c, \gamma') << 1$, we obtain

$$\left\{ g_0' \left[1 + \left(\frac{2}{\Delta\omega_0} \right)^2 \frac{d^2}{dt^2} \right] - \gamma_c - \gamma' + \gamma' \frac{|A|^2}{I_s} \right\} A(t) = 0. \tag{3-5}$$

By solving Equation (3-5), we can obtain the amplitude of the electric filed

$$A(t) = \frac{A_0}{\cosh(t/\tau_p)}, \tag{3-6}$$

where

$$\tau_p = \sqrt{\frac{2g_0'}{\gamma'}} \frac{2}{\Delta\omega_0} \sqrt{\frac{I_s}{|A_0|^2}}, \tag{3-7}$$

with g_0' being such that

$$\gamma_c + \gamma' - g_0' = \frac{4g_0'}{\Delta^2 \omega_0 \tau_p^2}. \tag{3-8}$$

This solution indicates that the saturable absorber inside the laser cavity will eventually cause the laser being pulsed in the form of hyperbolic secant.

3.2 Figure-eight laser

Figure-eight laser (F8L) was firstly introduced by Duling III [Dul91] in 1991. The name came from the unique shape of this type of fiber ring laser. In his paper, Duling III utilized an NALM as a mode-locker to generate passively mode-locked laser pulses. Those pulses were almost transform-limited with pulse-width as short as 2.1 ps. Shortly after, Richardson et al. [Ric91b] reported 320 fs soliton that was also generated by an F8L with an NALM. But the pulses had a slightly larger time-bandwidth product, which indicated a larger frequency chirping. The disadvantage of an F8L based on an NALM is that it needs an amplifier in the nonlinear loop to break the symmetry of the optical loop mirror. To overcome this disadvantage, F8Ls based on an NOLM were also investigated [Wu93]. However, the efficiency of NOLM-based F8Ls is less than that of the F8L using an NALM [Seo02]. The reason is that

when using a 50/50 coupler, the NALM can provide higher extinction ratio than NOLM.

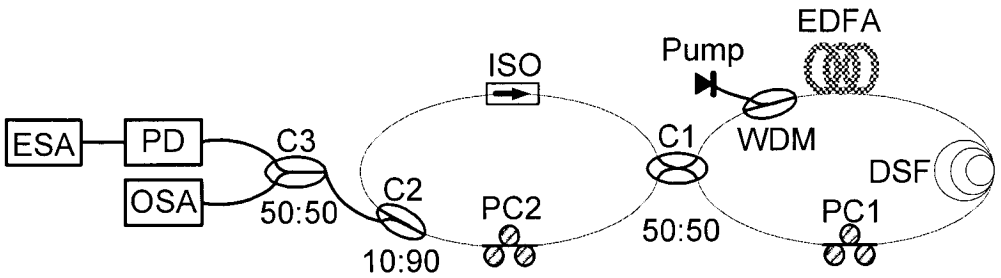

Fig. 3-2. Schematic diagram of an F8L using an NALM. ESA: electrical spectrum analyzer, PD: photodetector, OSA: optical spectrum analyzer, C1, C2, C3: couplers, ISO: isolator, PC1, PC2: polarization controllers, WDM: wavelength division multiplexer, EDFA: erbium-doped fiber amplifier, DSF: dispersion shifted fiber.

Fig. 3-2 shows the experimental setup of the F8L using an NALM. A 200-mW 1480-nm pumping LD made by FITEL is used to pump the EDF in the loop mirror through a 1480/1550 nm wavelength division multiplexer (WDM). The EDF (CorActive EDF-L4000-HCO) is 5-meter long. A 20-meter long DSF (Corning MetroCor) is used as a nonlinear device. A 3-dB coupler (C1) connects the nonlinear amplifying fiber loop with the linear loop, in which an optical isolator (ISO) is incorporated to ensure unidirectional operation of the linear loop. Two polarization controllers (PC1 and PC2) are used with each in one fiber loop to control the polarization state. The

laser output is obtained from the 10% port of the 10:90 coupler (C2). The output light is then equally divided by another 3-dB coupler (C3), with its optical spectrum monitored by an optical spectrum analyzer (OSA) and its electrical spectrum monitored by an electrical spectrum analyzer (ESA). An oscillator is also used to monitor the pulse train of the mode-locked laser.

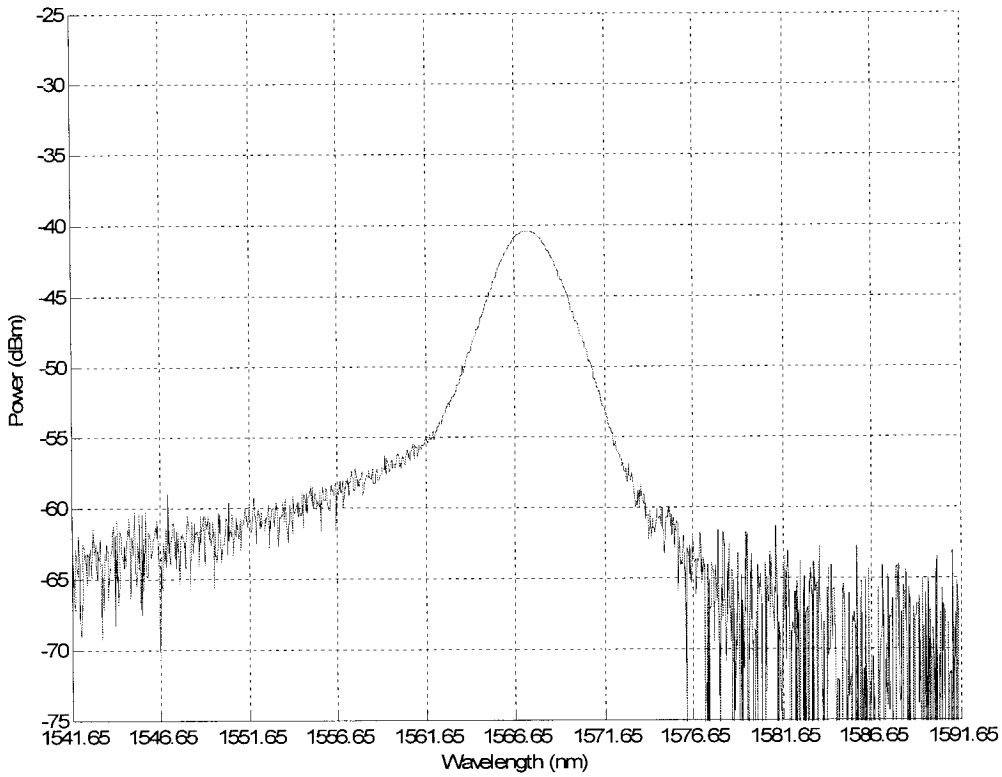

Fig. 3-3. Optical spectrum of the mode-locked laser.

The pumping power is 41.2 mW.

Fig. 3-3 shows the optical spectrum generated by the passively mode-locked laser. The central wavelength is at 1567.4 nm, with the full width at half maximum (FWHM) of 3.40 nm.

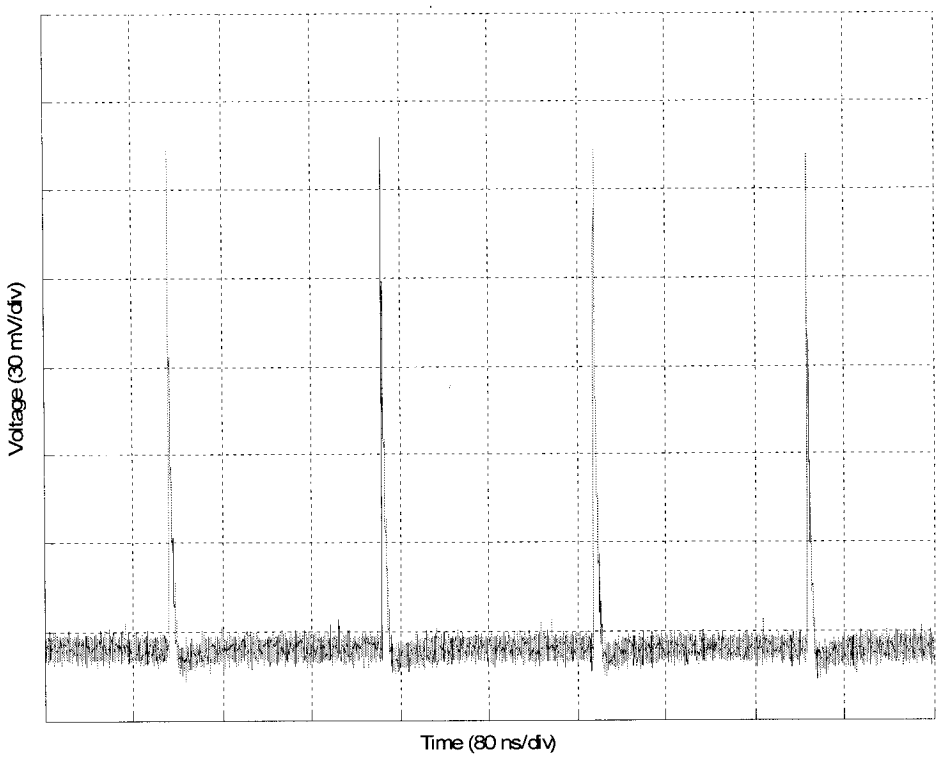

Fig. 3-4. Pulse train generated by the passively mode-locked fiber ring laser.

Fig. 3-4 shows the pulse train generated by the mode-locked laser measured by the oscilloscope. As can be clearly seen a stable optical pulse train is generated. The

spacing between two adjacent optical pulses is measured to be 191.6 ns, which corresponds to a repetition rate of 5.219 MHz. The repetition rate is determined by the total laser ring cavity length and is given by

$$f_R = \frac{c}{nL}, \tag{3-9}$$

where f_R is the pulse repetition rate, c is the light velocity in vacuum, n is the effective refractive index of the laser ring, L is the total length of the laser ring. From this equation, we can calculate that the total length of this F8L should be about 39.70 m.

3.3 Soliton in figure-eight laser

As the optical pulses generated by a mode-locked laser propagate inside the laser cavity, the pulses will eventually evolve into optical solitons. Therefore, we will give a detailed analysis on soliton in this section.

3.3.1 Fundamental optical soliton

Optical soliton can be described by the famous nonlinear Schrödinger (NLS) equation

$$-j\frac{\partial u}{\partial z} = -\frac{s}{2}\frac{\partial^2 u}{\partial t^2} + N^2|u|^2 u, \tag{3-10}$$

where $u(z,t)$ is the envelope function for the electrical field of the pulse, z is the propagation distance along the fiber, s=+1 or -1 is the sign of the group velocity dispersion (GVD) parameter β_2, and N is an integer presenting the order of the soliton.

The two terms in the right-hand part of Equation (3-10) can be further explained as following:

- The first term, $-\frac{s}{2}\frac{\partial^2 u}{\partial t^2}$, is attributed to the GVD effect of the fiber. It is well-known that this effect by itself will broaden the pulses in the time domain.
- The second term, $N^2|u|^2 u$, is a nonlinear item which represents the Kerr effect (the refractive index of the fiber will increase by a value proportional to the square of the electrical field of the light). Through the self-phase-modulation process, this effect will broaden the pulses in the frequency domain.

Equation (3-10) is a special class of nonlinear partial differential equation which can be analytically solved with a mathematical technique known as the inverse scattering

method [Zak72]. Both cases, $s=+1$ (normal dispersion) and $s=-1$ (anomalous dispersion), have been solved. According to the results, the pulse-like solutions, which correspond to solitons, only exist in the case of the anomalous dispersion. In the case of normal dispersion, the solutions to Equation (3-10) are sets of dips in a constant-intensity background. On the analogy of the previous case, these solutions are referred to as dark solitons which can find applications in the areas such as switching and guiding of light beams [Has95]. However, this type of special soliton is too complex in mathematics and is beyond the scope of this thesis. Therefore, only the case of anomalous dispersion ($s=-1$) will be discussed here. The NLS equation then has the form as

$$j\frac{\partial u}{\partial z}+\frac{1}{2}\frac{\partial^2 u}{\partial t^2}+N^2|u|^2 u=0. \tag{3-11}$$

At first let us consider the case of $N=1$, which presents the fundamental soliton. It is easy to show that the solution to Equation (3-11) under this situation is

$$u(z,t)=\mathrm{sech}(t)\exp(jz/2), \tag{3-12}$$

where *sech(t)* is the hyperbolic secant function. Obviously, this solution stands for a bell-shaped pulse whose amplitude is independent of propagating distance z. This is indeed the most valuable feature of soliton as well as the reason why optical soliton communication has attracted so many researchers.

In order to acquire a better understanding on how the optical soliton can keep its shape in the time domain even with dispersive transmission medium, it is helpful to prove this property from a more physical point of view. Consider an optical pulse $E=\cos(\omega t)$ propagating from $z=0$ along the $+z$ direction. After a distance of z, the pulse with a phase retardation φ can be written as

$$E=\cos(\omega t+\varphi)=\cos(\omega t-\beta z), \tag{3-13}$$

where ω is the angular frequency, β is the propagation constant. By using Taylor series, Equation (3-13) can be expended as

$$E=\cos(\omega t+\varphi)\approx\cos\left(\omega t+\varphi_0+t\frac{d\varphi}{dt}\right)=\cos\left[\left(\omega+\frac{d\varphi}{dt}\right)t+\varphi_0\right], \tag{3-14}$$

where the derivative $\frac{d\varphi}{dt}$ presents the frequency shifting for the optical pulse. It can be expressed as

$$\frac{d\varphi}{dt}=\frac{d(-\beta z)}{dt}=\frac{d}{dt}\left(-\frac{2\pi fn}{c}z\right)=-\frac{\omega z}{c}\frac{dn}{dt}, \tag{3-15}$$

where f is the frequency of the optical pulse, c is the velocity of light in vacuum, n is the refractive index of the fiber. Without considering the nonlinear effect, $\frac{dn}{dt}$ equals zero, which means there is not any frequency shifting. In this situation, the dispersion of the fiber will broaden the optical pulse in the time domain.

When the intensity of the optical pulse is large enough so that the nonlinearity cannot be ignored, something interesting happens. In this case, the Kerr effect must be taken into account

$$n = n_0 + n_2 I, \tag{3-16}$$

where n_0 is the original refractive index, n_2 is the nonlinear-index coefficient, which varies from 2.2×10^{-8} to $3.4\times10^{-8}\ \mu m^2/W$ for silica [Sut96], and I is the intensity of the optical pulse. Substituting Equation (3-16) into Equation (3-15), we can get

$$\frac{d\varphi}{dt} = -\frac{\omega z}{c}\frac{dn}{dt} = -\frac{\omega z}{c}\frac{d}{dt}(n_0 + n_2 I) = -n_2\frac{\omega z}{c}\frac{dI}{dt}. \tag{3-17}$$

For the different parts of an optical pulse, the changing of intensity $\frac{dI}{dt}$ has different signs. As shown in Fig. 3-5, for the leading edge of an optical pulse, $\frac{dI}{dt}$ is positive, whereas it changes to be negative for the trailing edge of that optical pulse. Consequently, the frequency shifting $\frac{d\varphi}{dt}$ for different part of an optical pulse has different signs. For the leading edge of an optical pulse, this frequency shifting is negative, which indicates a red-shift (shift to a lower frequency) effect. On the contrary, for the trailing edge of that optical pulse, the frequency shifting is positive, which indicates a blue-shift (shift to a higher frequency) effect.

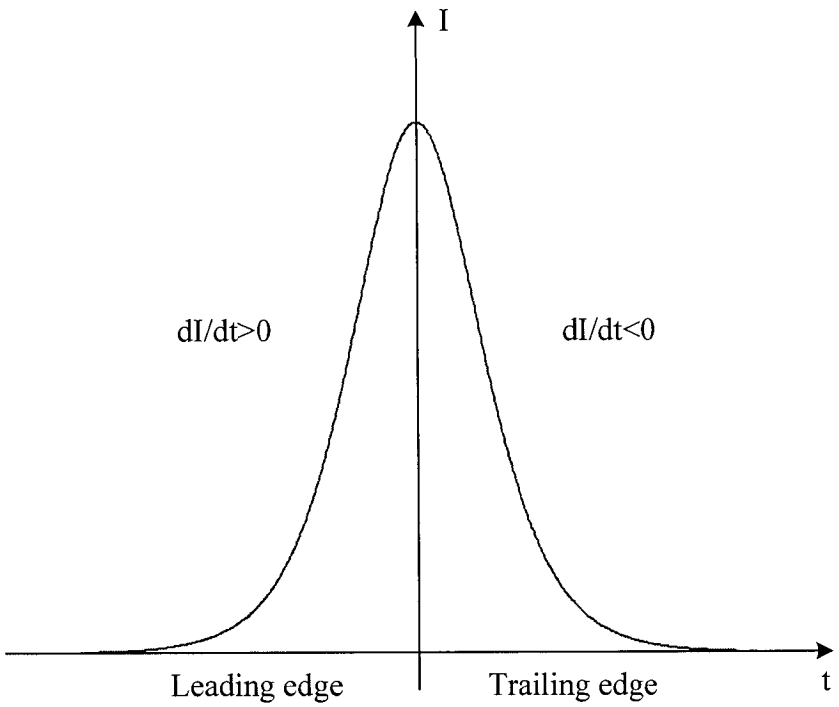

Fig. 3-5. Different intensity changing for an optical pulse.

Applying this result to the propagation of an optical pulse in a dispersive medium, we can find that the frequency shifting for the wings of the optical pulse will in turn change the shape of the optical pulse in the time domain. In the anomalous dispersion medium, the group velocity for higher frequency component is larger than that for the lower frequency component. Therefore, in an anomalous dispersion fiber, the red-shifted leading edge of an optical pulse will propagate more slowly, while the blue-shifted trailing edge of that optical pulse will propagate faster. Obviously, the result of this difference in group velocity is the shrink of the optical pulse in the time

domain. This shrink of pulse-width is caused by both the nonlinearity and the anomalous dispersion of the fiber for optical pulse with sufficiently strong intensity. It is not difficult to imagine that under certain conditions, this effect of pulse-shrinking can exactly cancel the effect of pulse-broadening caused by group velocity dispersion. When this happens, the optical pulse will propagate in the fiber without any distortion in its shape. That is exactly what Equation (3-12) indicates.

On the other hand, for the normal dispersion medium, it is easy to understand that the nonlinearity and the normal dispersion of the fiber will cause broadened optical pulse. Apparently, this pulse-broadening effect plus another pulse-broadening effect caused by group velocity dispersion cannot maintain the pulse shape as in the above situation. This result coincides with the conclusion we drew above that the pulse-like soliton solution to Equation (3-10) exists only when $s=-1$, which stands for anomalous dispersion.

Another important property of optical soliton, in addition to its anti-distortion property, is the self-evolving property. In a soliton system, even though the initial pulse may not have the hyperbolic secant shape, it will self-evolve in an attempt to become a soliton while it propagates in the system. Eventually, this pulse will attain the exact hyperbolic secant shape after a propagation distance long enough. It is this interesting property that determines the mode-locked optical pulses in an F8L will

evolve into optical solitons eventually. Fig. 3-3 presents a fundamental soliton generated in our experiments.

3.3.2 High-order optical soliton

Through the above description, we can gain a clear understanding on the fundamental soliton, which corresponds to the solution to Equation (3-11) under the condition $N=1$. Now the question is: what is the solution when $N>1$?

Further study of soliton theory shows that when $N>1$, the soliton pulse will experience periodic changes in its shape in time domain while it propagates along the fiber. The period for this type of shape-changing is defined as soliton period, which is in the order of hundreds of kilometers for a typical fiber transmission system. Another feature of high-order soliton is that it changes not only in its shape, but also in its spectrum, i.e. frequency chirping is introduced periodically to the soliton. Compared to the fundamental soliton which will keep its shape in both time domain and frequency domain when it propagates along the fiber, the high-order soliton is usually not preferable because of its frequency chirping.

One effective method to prevent the generation of high-order soliton is to reduce the soliton power. By examining the definition of the parameter N, one can find that its square is proportional to the peak power of the pulse. Therefore, a practical soliton system is usually operating in the situation that the pumping power is just above the threshold. In this way, one can ensure the stable operation of fundamental soliton and avoid the possibility of high-order soliton as well.

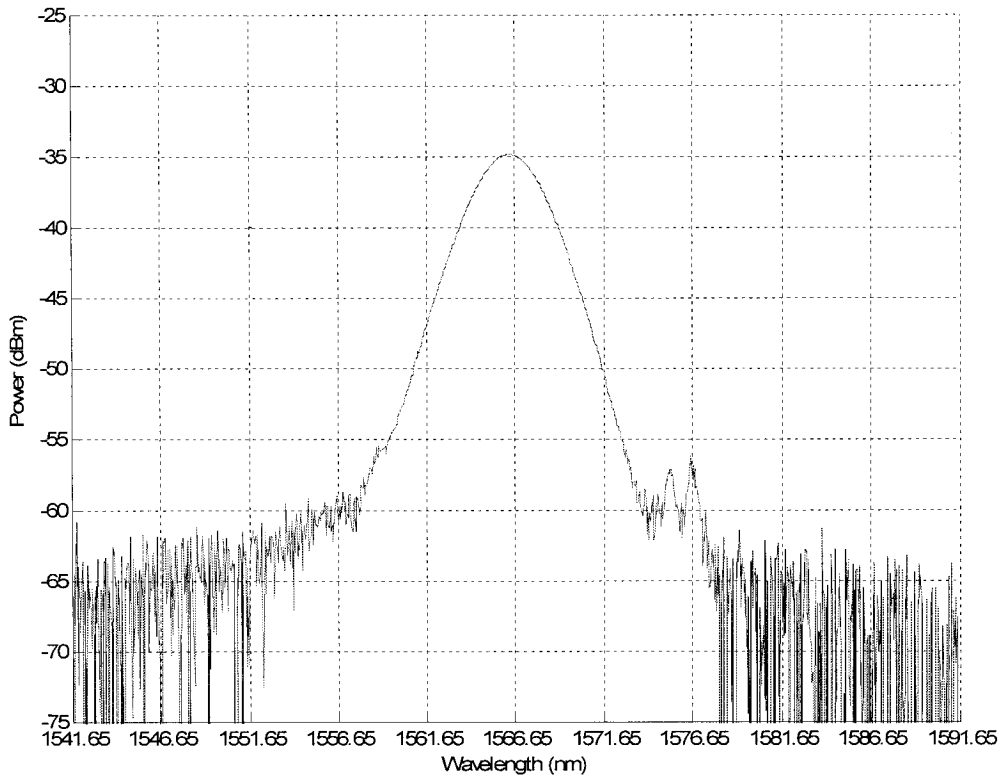

Fig. 3-6. Optical spectrum of high-order soliton when the pumping power is 53.6 mW.

Fig. 3-6 shows the optical spectrum of the high-order soliton occurred in our F8L experiment. The pumping power for this case was estimated to be 53.6 mW. Two small peaks on the right-wing and the left-wing can be clearly observed, which indicates that high-order solitons are generated.

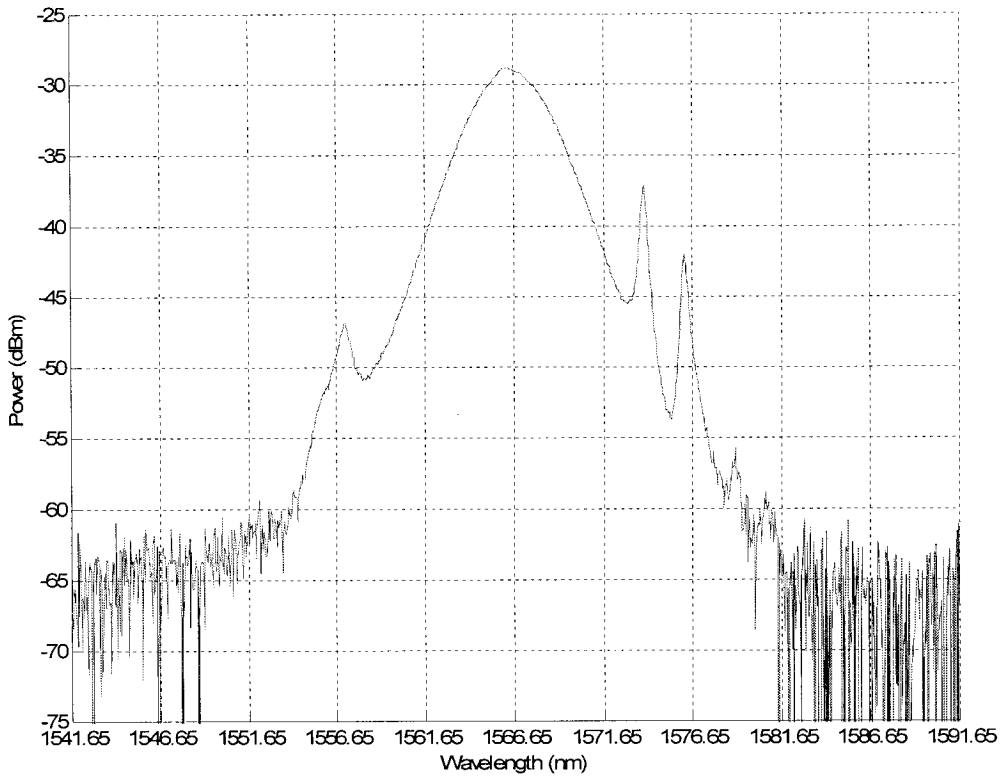

Fig. 3-7. Optical spectrum of high-order soliton

when the pumping power is 66.1 mW.

When the pumping power is further increased to around 66.1 mW, the high-order solitons become stronger, and more high-order solitons are stimulated. Fig. 3-7 shows the optical spectrum for this situation. Comparing to Fig. 3-6, one can find that the peaks on both wings of the laser become stronger, and two new small peaks emerge as well.

In the experiment, the pumping power is decreased to about 41.2 mW to suppress those peaks on both wings of the laser. This value is just slightly above the threshold for stable passive mode-locking. In this case, stable fundamental optical soliton is obtained.

3.4 Beating of the passively mode-locked laser for microwave signal generation

When a mode-locked laser output is applied to a photodetector, beating between different longitudinal modes of the laser will happen and a series of new frequency components will be generated. This process can be mathematically expressed as following.

According to the theory of mode-locking, the phases of all the longitudinal modes in a mode-locked laser are locked to be identical. The electric field of a mode-locked laser can be written as

$$E(t) = \sum_{p=0}^{N} A_p \cos[2\pi(f_0 + p \cdot f_c)t + \theta_0], \tag{3-18}$$

where $p = 0 \sim N$ stands for different longitudinal modes, f_c is the frequency spacing between adjacent modes, A_p, $f_0 + p \cdot f_c$, and θ_0 are amplitudes, frequencies, and phase of each longitudinal mode respectively. Note that here all the longitudinal modes have the same phase θ_0.

A photodetector is a square-law device. Therefore, by applying the output of a mode-locked laser to a photodetector, the output photo-current from the photodetector can be expressed as

$$\begin{aligned} i \propto E^2(t) &= \left\{ \sum_{p=0}^{N} A_p \cos[2\pi(f_0 + p \cdot f_c)t + \theta_0] \right\}^2 \\ &= \sum_{p=0}^{N} A_p^2 \cos^2[2\pi(f_0 + p \cdot f_c)t + \theta_0] + \\ &\quad \sum_{m<n} A_m A_n \{\cos[2\pi(2f_0 + (m+n)f_c)t + 2\theta_0] + \cos[2\pi(n-m)f_c t]\} \end{aligned} \tag{3-19}$$

From Equation (3-19), it is clearly seen that microwave signals at the frequencies of $k \cdot f_c$ ($k=1, 2, \ldots$) will be generated. Because all the longitudinal modes have the exactly same phase, their phase fluctuation will then be cancelled by each other when beating happens. Therefore, the generated microwave signal can have very low phase noise, and consequently very narrow line-width. It should be noted that the frequency components of $f_0 + p \cdot f_c$ and $2f_0 + (m+n)f_c$ are considerably higher than the cut-off frequency of the photodetector, therefore they cannot be observed. Only part of the frequency components $(n-m)f_c$ that are below the cut-off frequency of the photodetector can be detected. Here f_c is the frequency spacing between adjacent modes and is given by

$$f_c = \frac{c}{nL}, \tag{3-20}$$

where c is the light velocity in vacuum, n is the effective refractive index, L is the cavity length.

One important application for the beating of mode-locked fiber laser is photonic generation of microwave signal. Microwave signals are conventionally generated using electronics by multiplying a low frequency to a high frequency with several stages of multipliers and amplifiers. Consequently, the system is bulky, complicated, and inefficient with high phase noise. By utilizing the beating signal, photonic generation of microwave or millimeter wave signals is considered a promising

alternative to overcome these drawbacks. According to the above analysis, the beating signal of the mode-locked laser will generate microwave signals with very high quality. Therefore, the experiment to generate microwave signal using the F8L has been implemented in this project.

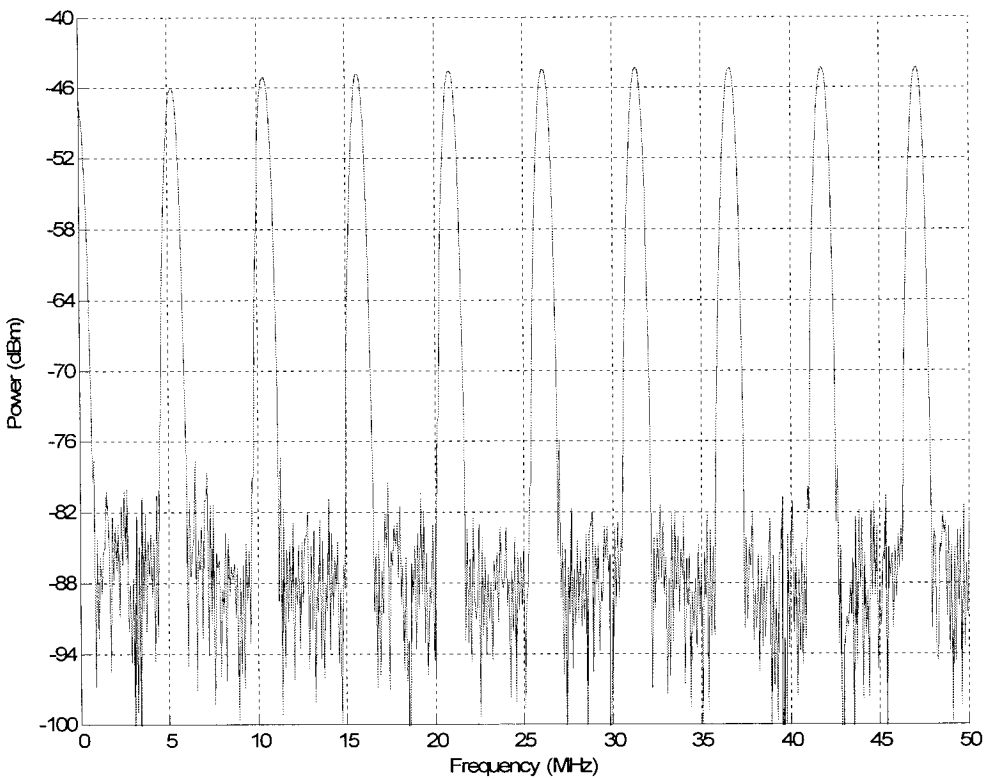

Fig. 3-8. Beating signals generated by the passively mode-locked fiber ring laser.

In this experiment, the mode-locked lasing output from the F8L is applied to a 25-GHz photodetector (New Focus, model 1414), and the output signal from the photodetector is then monitored by a spectrum analyzer (Agilent E4448A). Fig. 3-8 shows the spectrum of the beating signals obtained at the output of the photodetector. It can be confirmed from this figure that a series of microwave signals are generated. Their frequencies are all at the harmonics of 5.25 MHz. According to Equation (3-19), the frequency spacing between adjacent longitudinal modes is thus determined as 5.25 MHz. By taking this value and $c = 3\times10^{8} m/s$, n=1.47 into Equation (3-20), the total length of the cavity of our F8L can be calculated as about 38.87 m.

Fig. 3-9 shows a zoom-in spectrum of the beating signal at 5.25 MHz. From this figure, it is clearly seen that the linewidth of the beating signal is as narrow as around 1 Hz. The sidelobe suppression ratio is as high as about 70 dB. With these measurements, one can draw the conclusion that the phase noise of the beating signal is very low. This should be accredited to the very good coherence between longitudinal modes of the passively mode-locked fiber ring laser.

The results of above experiment confirm that passively mode-locked fiber laser can generate very high quality microwave signal. However, the frequency of these signals is usually as low as only several MHz, so that these signals cannot find practical applications. This problem will be solved in chapter 5 of this thesis.

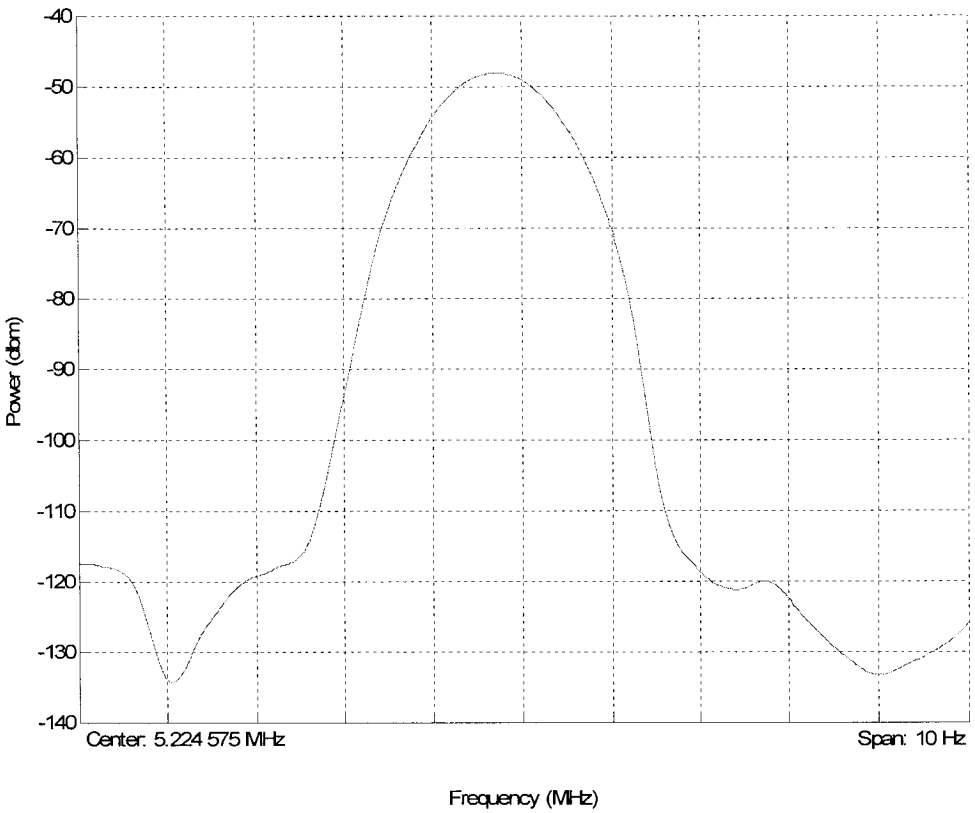

Fig. 3-9. Zoom-in spectrum of the beating signal at 5.22 MHz.

3.5 Summary

The theory of passive mode-locking using a saturable absorber was examined in this chapter. An F8L using an NALM was then built and experimentally demonstrated. The theory of soliton was briefly discussed. The optical pulses in the passively mode-

locked F8L were confirmed to evolve into optical solitons. The method to avoid high-order soliton operation of an F8L was also suggested. An important application of the proposed passively mode-locked fiber ring laser is to generate high-quality microwave signals. It was demonstrated by applying the output of the passively locked F8L to a photodetector, stable high-quality microwave signals were generated.

Chapter 4 Multiwavelength passively mode-locked fiber ring laser

Multiwavelength optical pulses have applications in many fields. They can be generated by either active mode-locking or passive mode-locking. However, the configuration of multiwavelength actively mode-locked laser is complicated because the round-trip length for all the wavelengths must be identical. Therefore, the multiwavelength passive mode-locking is investigated is this chapter. A simple configuration of passively mode-locked fiber ring laser with multiple cascaded FBGs as the wavelength selector is proposed.

4.1 Fiber Bragg grating

Since the invention in 1978 by Hill [Hil78] at the Communications Research Centre, Ottawa, Canada, fiber Bragg gratings (FBG) have been becoming the most widely used passive components in fiber-optic systems serving as optical filters. In this section, a passively mode locked fiber ring laser to achieve multiwavelength lasing using cascaded uniform FBGs is proposed and experimentally demonstrated. Since

the cascaded FBGs in the fiber ring are the key components in wavelength selection, in this section we will discuss briefly the fundamentals of FBGs.

An FBG is a segment of optical fiber with periodic variations in the refractive index along the fiber. Light launched into an FBG that satisfying the Bragg condition will be reflected. Therefore, an FBG is usually used as a reflection optical filter.

FBGs can be fabricated using two different techniques: phase mask technique and holographic technique. The most widely adopted technique, especially for the commercial purpose, is the phase mask technique. Fig. 4-1 shows the principles of the phase mask technique. A strong UV laser beam illuminates the stripped bare fiber through a specially designed phase mask. This phase mask itself is a precisely manufactured diffractive grating, which is usually a thin flat piece of glass with a pattern of fine parallel troughs etched on one side. The phase mask is designed in such a manner that most of the incident UV beam will be diffracted by it into the ± 1 order diffracted beams. These two beams then interfere with each other and an interference pattern is formed at the core of the bare fiber.

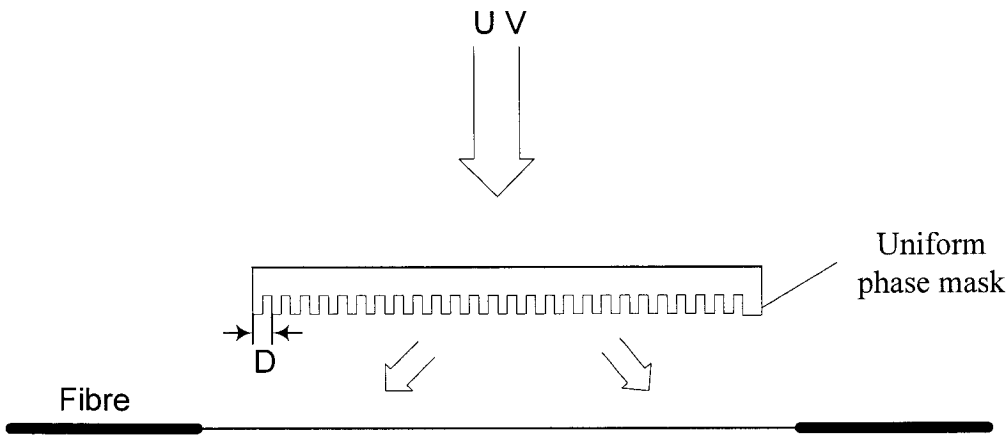

Fig. 4-1. FBG fabrication with the phase mask technique.

The refractive index change induced by the interference pattern can be expressed as

$$\delta n_{eff}(z) = \bar{\delta} n_{eff}(z)\left\{1 + v\cos\left[\frac{2\pi}{\Lambda} z + \phi(z)\right]\right\}, \tag{4-1}$$

where $\bar{\delta} n_{eff}$ is the "DC" index changing, v is the fringe visibility of the index changing, Λ is the period of the index change, and $\phi(z)$ is the grating chirping. By using the coupled-mode theory, one can calculate the amplitude and power reflection coefficients ρ and r for such an FBG [Erd97]

$$\rho = \frac{-\kappa \sinh\left(L\sqrt{\kappa^2 - \hat{\sigma}^2}\right)}{\hat{\sigma}\sinh\left(L\sqrt{\kappa^2 - \hat{\sigma}^2}\right) + j\sqrt{\kappa^2 - \hat{\sigma}^2}\cosh\left(L\sqrt{\kappa^2 - \hat{\sigma}^2}\right)}, \tag{4-2}$$

$$r = |\rho|^2 = \frac{\sinh^2\left(L\sqrt{\kappa^2 - \hat{\sigma}^2}\right)}{\cosh^2\left(L\sqrt{\kappa^2 - \hat{\sigma}^2}\right) - \frac{\hat{\sigma}^2}{\kappa^2}}, \tag{4-3}$$

where κ is an "AC" coupling coefficient, L is the length of the grating, and $\hat{\sigma}$ is defined by

$$\hat{\sigma} = \delta + \sigma - \frac{1}{2}\frac{d\phi}{dz}, \tag{4-4}$$

in which

$$\delta = \beta - \frac{\pi}{\Lambda}, \tag{4-5}$$

$$\sigma = \frac{2\pi}{\lambda}\bar{\delta}n_{eff}, \tag{4-6}$$

where λ is the wavelength in vacuum, $\beta = (2\pi/\lambda)n_{eff}$ is the mode propagation constant.

4.2 Multiwavelength passively mode-locked fiber ring laser using cascaded FBGs

Multiwavelength optical pulses are attractive to applications such as wavelength-division-multiplexed (WDM) communication systems, fiber optic sensing, and optical signal processing. Mode-locking is one of the most widely used techniques in generating narrow optical pulses. Both active [Bak99] and passive [Ric91a] mode-locking have been developed in the past years.

For active mode locking, an optical intensity modulator is usually used in the laser cavity to force the oscillating longitudinal modes to maintain a fixed phase relationship with each other. Multiwavelength active mode locking can also be implemented, but the round-trip frequencies for all the wavelengths must be identical [Li99], which makes the implementation very complicated. Recently, Yao et al. proposed a method to achieve multiwavelength active mode locking using a sampled fiber Bragg grating (SFBG) [Yao01]. Considering that the reflection locations for all the wavelengths at an SFBG are the same, fiber lasers using an SFBG can achieve multiwavelength active mode locking with identical roundtrip frequencies. However, to obtain very narrow optical pulses by active mode locking requires very high-speed intensity modulator and a high-frequency microwave source, which make the actively mode-locked fiber lasers very complicated and costly.

Passive mode locking has been considered a promising alternative for narrow optical pulse generation. Without a high-speed intensity modulator and a high-frequency microwave source, passively mode-locked lasers are much less complex than active mode-locked lasers. A few demonstrations have been suggested to achieve dual-wavelength passive mode-locking [Nos94], [Okh00]. In [Nos94], a 3-dB coupler with two FBGs that have two different center reflection wavelengths were connected to each arm of the 3-dB coupler was incorporated in the laser cavity. With this configuration, the round-trip lengths for the two wavelengths were maintained identical. Dual-wavelength passive mode locking was realized.

However, to maintain an equal round-trip length for all the wavelengths makes the configuration of a mode-locked laser very complicated. In addition, it is very difficult to achieve if the number of wavelengths is more than two. To solve this problem, in this thesis we investigate the mechanism of passive mode-locking and find that the round-trip lengths for different wavelengths are not necessarily identical if the laser is passively mode locked. In this chapter, a multiwavelength passively mode locked fiber ring laser by cascading multiple FBGs in the laser cavity serving as wavelength selection component is built. The laser has a figure-of-eight structure with an NALM incorporated in the fiber ring as a saturate absorber. Since the locations of the cascaded FBGs are different, the lasing wavelengths have different round-trip lengths. Experimental results based on the proposed structure show that a stable multiwavelength passive mode locking with round-trip frequencies of 780 kHz, 855 kHz and 932 kHz for the three wavelengths is realized.

The experimental set-up is shown in Fig. 4-2. Three FBGs with center reflection wavelengths of 1553.3 nm, 1555.5 nm, and 1557.5 nm are incorporated into the fiber ring through an optical circulator for wavelength selection. The separation between two adjacent FBGs is 12 m. The reflection spectrum of the cascaded FBGs is shown in Fig. 4-3. The circulator in the fiber ring also serves as an isolator to maintain a unidirectional operation of the fiber ring. In the fiber ring, an 11-m long EDF pumped by a 980-nm semiconductor LD is used as the gain medium. To suppress the homogeneous broadening, the EDF is cooled in liquid nitrogen. The laser output is

obtained from the 10% port of a 10:90 coupler (C2). To monitor simultaneously the optical spectrum and the optical pulses, the output is further divided into two parts by a 3-dB coupler (C3). The optical spectrum is monitored by an optical spectrum analyzer. The optical pulses are obtained at a photodetector and displayed on an oscilloscope.

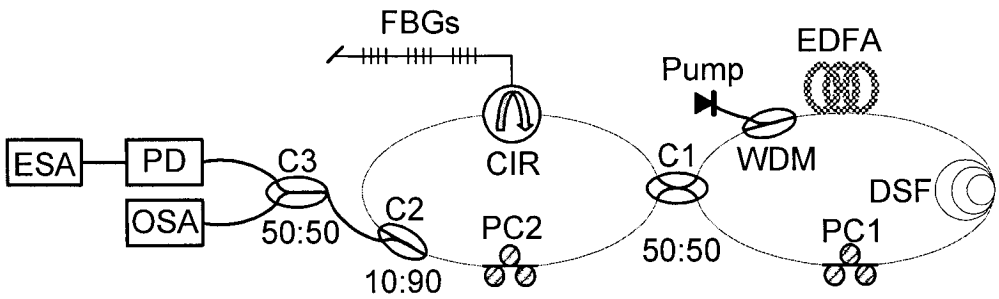

Fig. 4-2. Experimental setup of a multiwavelength passively mode-locked fiber ring laser. ESA: electrical spectrum analyzer, PD: photodetector, OSA: optical spectrum analyzer, C1, C2, C3: couplers, CIR: circulator, PC1, PC2: polarization controllers, WDM: wavelength division multiplexer, EDFA: erbium-doped fiber amplifier, DSF: dispersion shifted fiber.

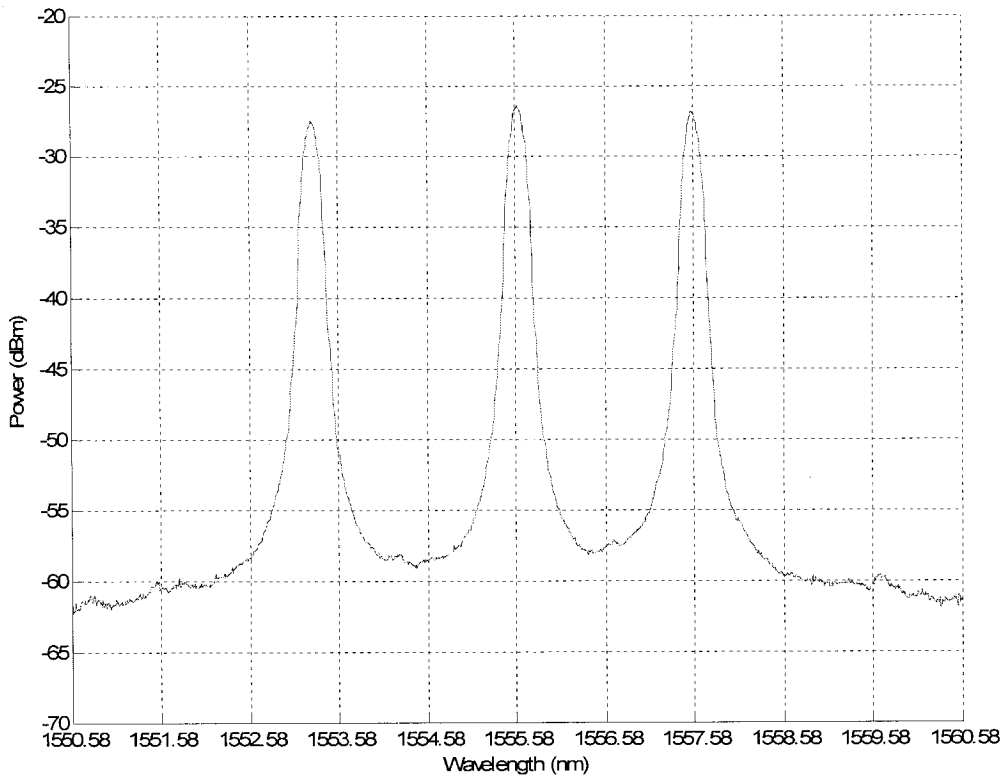

Fig. 4-3. Reflection spectrum of the three cascaded FBGs.

As discussed in Chapter 3, the NALM is the key component to achieve passive mode locking. The NALM in the proposed laser consists of an 11-meter long EDF pumped by a 250-mW 980-nm LD and a 200-m long DSF. The EDF is located more close to one port of the 50% coupler (C1) within the nonlinear ring to ensure an unbalanced nonreciprocal. The DSF has an effective area of $72\mu m^2$, which provides a much greater nonlinearity compared to conventional single mode fiber. The power transmittance of the NALM depends on the input intensity and is given by [Fer90]

$$T = \frac{P_t}{P_i} = G\sin^2\left[\frac{\pi n_2 L}{2\lambda}(G-1)I_i\right], \tag{4-7}$$

where P_i and P_t are the input and transmitted light power, I_i is the input light intensity, G is the gain of the EDFA, λ is the free-space wavelength of the light, n_2 is the Kerr coefficient, and L is the length of the DSF.

When $\frac{\pi n_2 L}{2\lambda}(G-1)I_i$ is small, Equation (4-7) can be approximated as

$$T \approx G^3\left(\frac{\pi n_2 L}{2\lambda} I_i\right)^2 \text{ or } T \propto I_i^2. \tag{4-8}$$

From Equation (4-8), we can see that the transmittance of the NALM is proportional to the square of input intensity. This indicates that the gain of the NALM for high intensity light is higher than that for small intensity light. Therefore, when a continuous wave (CW) laser light with small intensity fluctuation enters the NALM, the peak of the small fluctuation will be amplified more than the leading and trailing edges. The result of this intensity-dependent amplification is that the intensity difference between the peak and the edges increases every time the fluctuation passes the NALM. Eventually, the small intensity fluctuation of a CW laser will be amplified into a large intensity pulse by the NALM, and hereby the laser is passively mode-locked. In such a passive mechanism, it is the nonlinear property of the NALM that passively locks the phases of the longitudinal modes of the laser.

Referring to Equation (3-6) we can see that the electric field has the pulse shape of sech function, which is independent of the round-trip time or the cavity length. It is different from active mode locking where the round-trip frequencies for all wavelengths must be identical in order to actively mode lock the phases of the longitudinal modes. For passive mode locking, the round-trip frequencies are not necessarily identical. As a matter of fact, in the similar derivation for active mode-locking, the operator for round-trip evolution of electric field through the modulator $\hat{T}_m = 1 - \gamma_m(1 - \cos\omega_m t)$ is dependant on the modulating frequency ω_m, and the amplitude of the electric field will have a pulsed form only when the round-trip time equals to the multiples of the period of the modulation signal. It is this modulation frequency dependency of $\hat{T}_m$ that proposes additional restriction on active mode locking. For single wavelength operation, this additional restriction is satisfied by selecting suitable modulation frequency. For multiwavelength operation, this restriction must be satisfied for all wavelengths. A simple method to achieve this is to use an SFBG [Yao01], in which the reflection locations for all wavelengths are inherently the same. Fiber lasers using an SFBG can achieve multiwavelength active mode locking with identical round-trip frequency. Otherwise, a specially designed structure must be employed to ensure an identical round-trip length for all the wavelengths [Li99].

On the contrary, based on Equation (3-5) there is nothing related to the round-trip time or length for passive mode locking. In other words, with a saturable absorber used, passively mode-locked pulses will be formed without adjusting the round-trip lengths. Therefore, the adjustment of the round-trip time for multiwavelength passive mode-locking, such as the specially designed cavity structure in [Nos94], is not needed. A simple configuration that incorporates cascaded FBGs with different round-trip frequencies would be able to generate multiwavelength passively mode-locked optical pulses.

A multiwavelength passively mode-locked fiber ring laser with three cascaded FBGs shown in Fig. 4-2 is implemented. With careful adjustment of the polarization controllers (PC1 and PC2), the fiber ring laser is switched from CW operation to mode-locked operation, with all three wavelengths mode-locked simultaneously.

The optical spectrum of the generated multiwavelength passively mode-locked laser in our experiment is shown in Fig. 4-4. It can be seen that the three lasing wavelengths are at 1553.3 nm, 1555.5 nm, and 1557.5 nm, which are determined by the peak reflection wavelengths of the three FBGs.

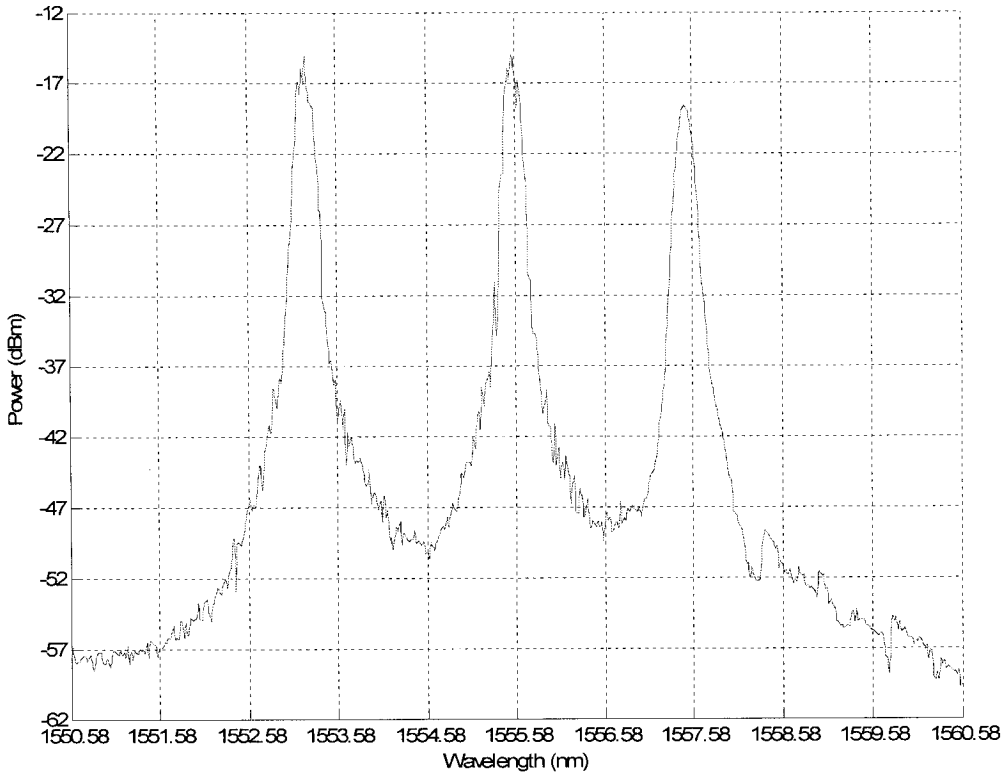

Fig. 4-4. The optical spectrum of the three-wavelength passively mode-locked fiber ring laser.

When the laser output is applied to a photodetector, beating signals between any two mode-locked longitudinal modes are generated. Refer to Equation (3-19), it is easy to see that the beating signal will have frequencies of $k \cdot f_c$ (k=1, 2,...) where $f_c = \frac{1}{T_{RT}}$ is the reciprocal of the round-trip time. For multiwavelength passive mode-locking,

since the three wavelengths are determined by the three cascaded FBGs with different round-trip time, the beating signals with different frequencies will be observed.

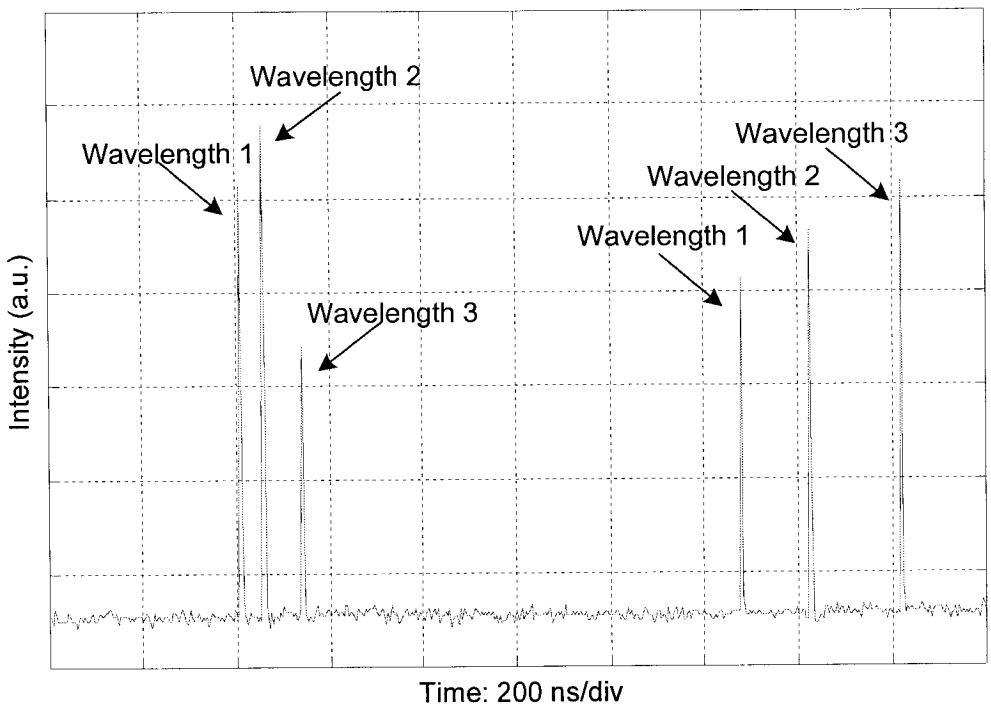

Fig. 4-5. The three pulse trains generated by the three-wavelength passively mode-locked laser.

Fig. 4-5 shows the pulse trains generated by the multiwavelength passively mode-locked fiber ring laser. It is clearly seen that three pulse trains which correspond to the three passively mode-locked wavelengths are generated. By measuring the time

intervals between pulses of wavelength 1, wavelength 2, and wavelength 3, we can determine that the repetition rates of the three wavelengths are 932 kHz, 855 kHz, and 780 kHz, respectively. These frequencies match the round-trip frequencies of the respective wavelengths very well.

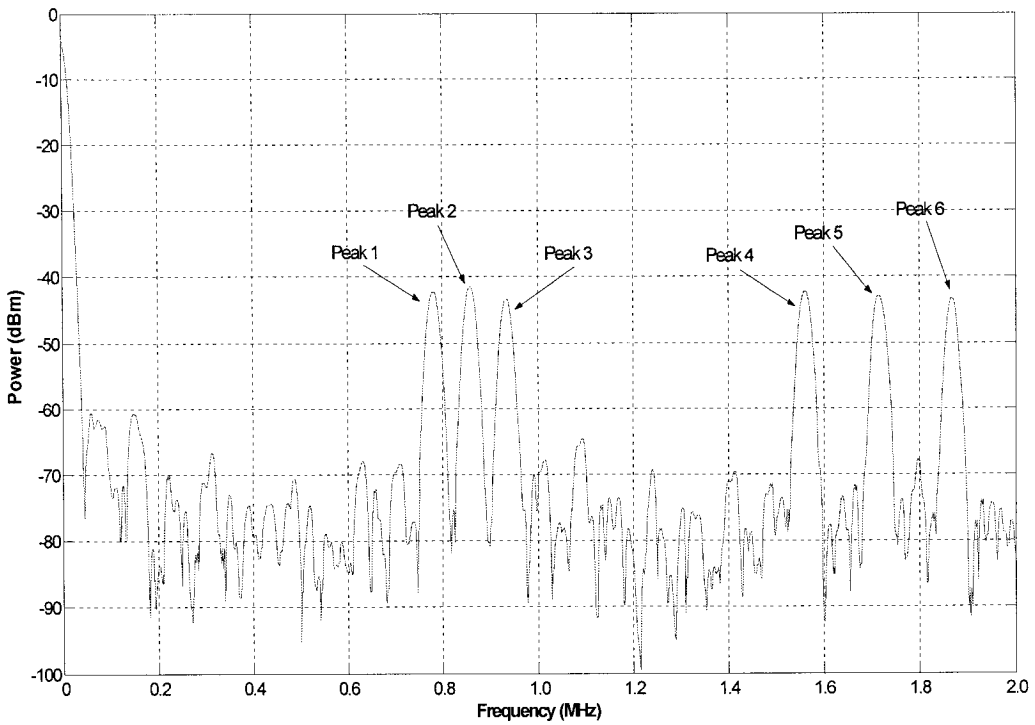

Fig. 4-6. The spectra of the beating signals of the three-wavelength passively mode-locked fiber ring laser.

Fig. 4-6 shows the electrical spectra of the beating signals generated by the multiwavelength passively mode-locked fiber ring laser. Peak 1 (780 kHz), peak 2 (858 kHz) and peak 3 (934 kHz) correspond to the frequency spacing between two adjacent longitudinal modes of the passively mode-locked laser for the three wavelengths. Peak 4 (1.560 MHz), peak 5 (1.716 MHz), and peak 6 (1.868 MHz) correspond to the second-order harmonics of the beating signals of the three wavelengths. The beating signals reveal that the passive mode locking is realized for the three wavelengths with different round-trip frequencies. Therefore, this experiment confirms that multiwavelength passive mode-locking can be established when the round-trip frequencies are different.

4.3 Summary

In this chapter, a multiwavelength passively mode-locked fiber ring laser was demonstrated. The laser was constructed based on the figure-of-eight structure with an NALM for passive mode locking. Three cascaded fiber Bragg gratings were used in the ring cavity for wavelength selection. The experiment showed that passive mode locking was achieved for the three wavelengths with different round-trip frequencies. The beating signals for the three wavelengths at 780 kHz, 858 kHz, and 934 kHz were observed which verified that the multiwavelength passive mode locking was realized with three different round-trip frequencies. With this method, passively

mode-locked laser with more wavelengths can be easily obtained by increasing the number of cascaded FBGs in the cavity.

Chapter 5 Rational harmonic actively mode locked fiber ring laser

The passively mode locked fiber ring laser discussed in Chapter 3 can be used to generate microwave signals at very low frequencies. This is because the laser has a long cavity length, which leads to a small longitudinal mode spacing. The beating between the mode-locked longitudinal modes can generate stable low phase noise microwave signals, but at very low frequencies. To generate microwave signals at high frequencies, in this chapter we propose to use rational harmonic actively mode-locked fiber ring laser to generate microwave signals. It is different from the passively mode locked fiber ring lasers, in which microwave signals can be generated by beating the mode-locked longitudinal modes with low microwave frequencies, the use of rational harmonic actively mode-locked fiber ring lasers can generate microwave frequencies at much higher frequency even with a very long ring cavity. To this end, a rational harmonic actively mode-locked fiber ring laser is implemented and a stable high-quality microwave signal by beating the actively locked rational harmonics is generated. In the proposed laser, the microwave signal used to drive the intensity modulator for active mode locking has a frequency of 5.5 GHz, the frequency of the generated microwave signal is 22 GHz, which means that the frequency of the generated microwave signal is four times the frequency of that of the modulating signal.

5.1 Photonic generation of microwave signal using a rational harmonic actively mode locked fiber ring laser

In chapter 3, we have demonstrated that microwave signals can be generated by the beating of the mode locked longitudinal modes of a passively mode-locked fiber ring laser. Since the length of the fiber laser is very long, the generated microwave signal has a low microwave frequency.

For a mode-locked laser, the frequency of the generated microwave signals is $k \cdot f_c$ (k = 1, 2, ...), where f_c is the cavity fundamental frequency determined by the optical length of the laser cavity. For a fiber ring laser, we have

$$f_c = \frac{c}{nL}, \tag{5-1}$$

where c is the light velocity in vacuum, n is the refractive index of the laser cavity, L is the length of the ring cavity. For a fiber ring laser, L is usually in the range of tens of meters and can hardly be reduced to a few meters, especially when an EDFA is used in the laser cavity to provide the gain. Therefore, f_c is very unlikely to be more than 20 MHz. This means that the frequencies of optically generated microwave signals using passively mode-locked fiber ring lasers are limited to several tens of MHz.

On the other hand, for active mode-locking, the frequency of the generated microwave signals is equal to the frequency of the RF signal applied to the modulator. This frequency must be carefully tuned to $k \cdot f_c$ ($k = 1, 2, \ldots$) so that mode locking can be established. With the assistance of a high-speed optical modulator, this RF frequency can be easily set to as high as several tens of GHz. Therefore, the generated microwave signal can have a frequency up to several tens of GHz, which is high enough for most applications. However, the use of a high-speed modulator will make the system very expensive. In addition, the currently commercially available electro-optic modulators can operate at a maximum frequency of about 40 GHz. For many applications, such as the next-generation broadband wireless access networks, the operating frequency is expected to be in the 60 GHz band. An active mode locked laser using electro-optic modulators cannot generate a microwave signal at 60 GHz band.

A solution to this problem is to use a rational harmonic actively mode-locked fiber laser to generate high-frequency microwave signals. Rational harmonic actively mode-locking fiber lasers have been investigated in recent years [Ono93]. It is different from a conventional harmonic actively mode-locked fiber laser; in a rational harmonic actively mode-locked fiber laser the modulating frequency f_m is slightly detuned from the exact harmonic of the laser cavity fundamental frequency f_c

$$f_m = \left(i + \frac{1}{j}\right) f_c, \tag{5-2}$$

where i is a positive integer, and j could be either positive or negative integer. It can be shown [Ahm96] that in this situation, the repetition rate of the mode-locked laser pulses is the lowest common multiple of the laser cavity resonance frequency and the RF modulation frequency, i.e. the repetition rate would be

$$f_p = |j| f_m = \left(i|j| \pm 1\right) f_c . \tag{5-3}$$

Therefore, by applying the optical pulses with a repetition rate of f_p to the photodetector, a microwave signal with a frequency $|j|$ times higher than the frequency of the modulating signal will be generated.

5.2 Rational harmonic actively mode-locked fiber laser

To generate a microwave signal at a high microwave frequency, a rational harmonic actively mode-locked fiber ring laser is built and experimented. The schematic diagram of the fiber laser is shown in Fig. 5-1. The frequency of the modulating signal used to drive the intensity modulator is 5.52 GHz. By carefully adjusting the PC, rational harmonic mode locking is established. By applying the output to a PD, a microwave signal resulted from the beating between the mode-locked rational

harmonics at 22.1 GHz is observed. The frequency of the generated microwave signal is four times higher than the frequency of the modulating signal. The spectrum of the generated microwave signal is shown in Fig. 5-2. The pulse train generated by the mode-locked laser is shown in Fig. 5-3.

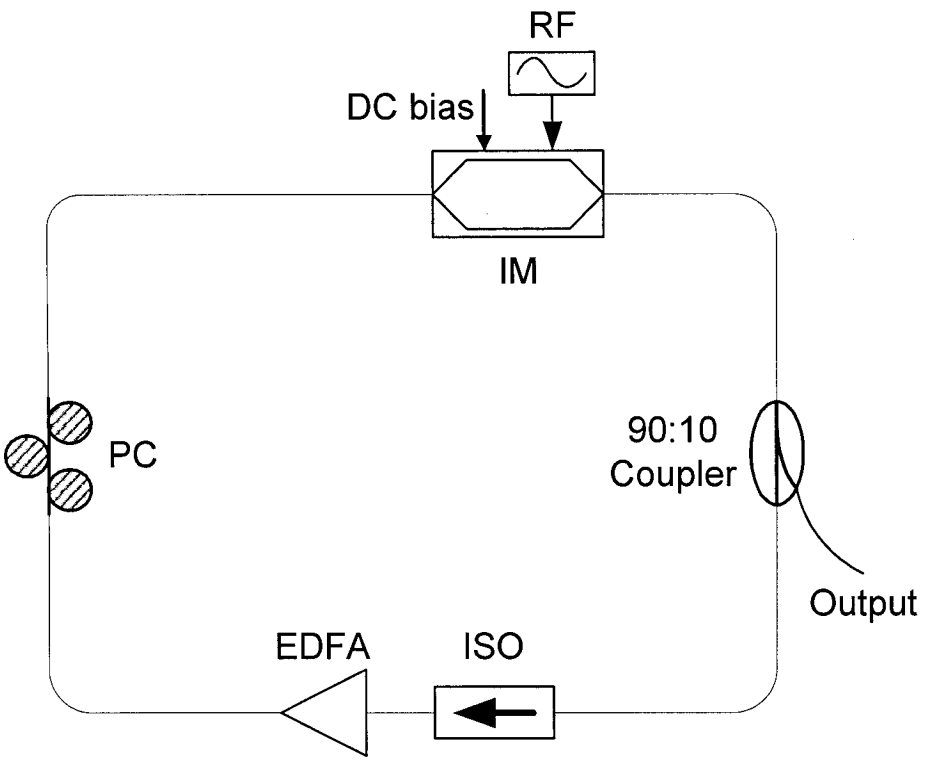

Fig. 5-1. Schematic diagram of the rational harmonic mode-locked ring laser. IM: intensity modulator, ISO: isolator, EDFA: erbium-doped fiber amplifier, PC: polarization controller.

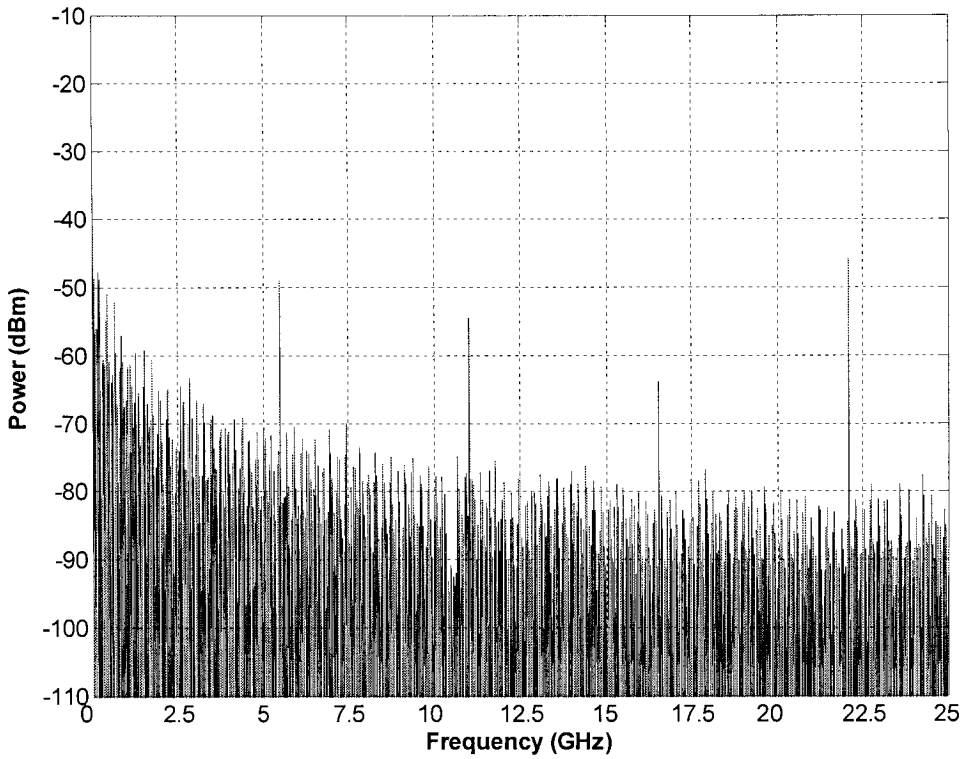

Fig. 5-2. The spectrum of the beating signal of

a fourth-order rational harmonic mode-locked fiber ring laser.

Based on Fig. 5-3, we can see that the amplitude of the pulse train is severely uneven. This is because the lower-order harmonic components have a relatively high power. As can be seen from Fig. 5-2, the power of the fundamental harmonic is only 3-dB lower than that of the fourth-order harmonic, and the power of the second- and third-order harmonics is also very high.

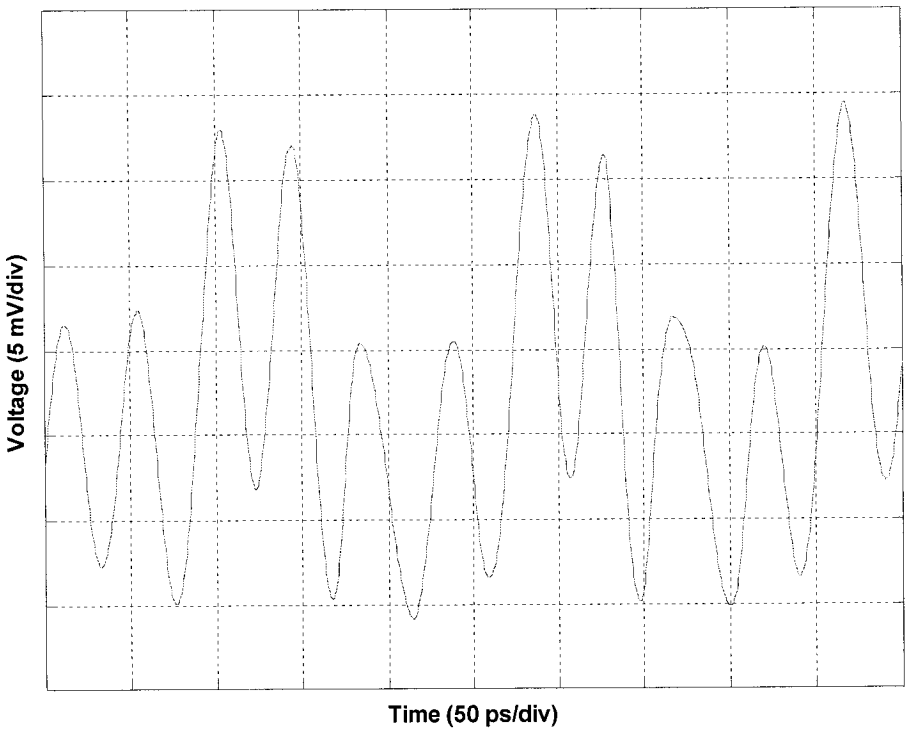

Fig. 5-3. Pulse train of the fourth-order rational harmonic mode-locked fiber ring laser.

The reason that the power of the output pulse train is not concentrated in the fourth-order harmonic is that in a rational harmonic mode-locked laser, the modulating frequency is not the same as the repetition rate of the optical pulses. Therefore, when different pulses reach the modulator, they will be at different timing point of the modulation period. This results in different loss for each pulse. Consequently, different pulses in the pulse train have different amplitude. This uneven amplitude

results in unexpected frequency components of the pulse train, which greatly degrade the quality of the generated microwave signal.

Several methods have been proposed to equalize the pulse amplitude, which include using a Fabry-Perot semiconductor modulator [Zha01], and using an SOA loop mirror [Tan03]. In the following sections, two of these methods are investigated in detail.

5.3 Amplitude equalization utilizing nonlinear polarization rotation

One method to equalize the pulse amplitude is to utilize the nonlinear polarization rotation (NPR) [Li01]. The schematic diagram of a rational harmonic mode locked fiber laser that using NPR to equalize the pulse amplitude is shown in Fig. 5-4. An EDFA provides the gain for the fiber ring laser. An isolator (ISO) ensures the unidirectional operation of the ring laser. The mode-locking of the laser is achieved by a $LiNbO_3$ intensity modulator which is modulated by an RF signal. The pulse amplitude equalizer consists of a polarizer, two polarization controllers (PC1 and PC2), and a section of DSF as the nonlinear fiber because of its small effective area. The polarizer can be adjusted to ensure the appropriate polarization state for the input light to the $LiNbO_3$ intensity modulator. A 90:10 coupler provides the 10% output

light, which is sent to a photodetector. The output electrical signal from the photodetector is then fed to an electrical spectrum analyzer and an oscilloscope.

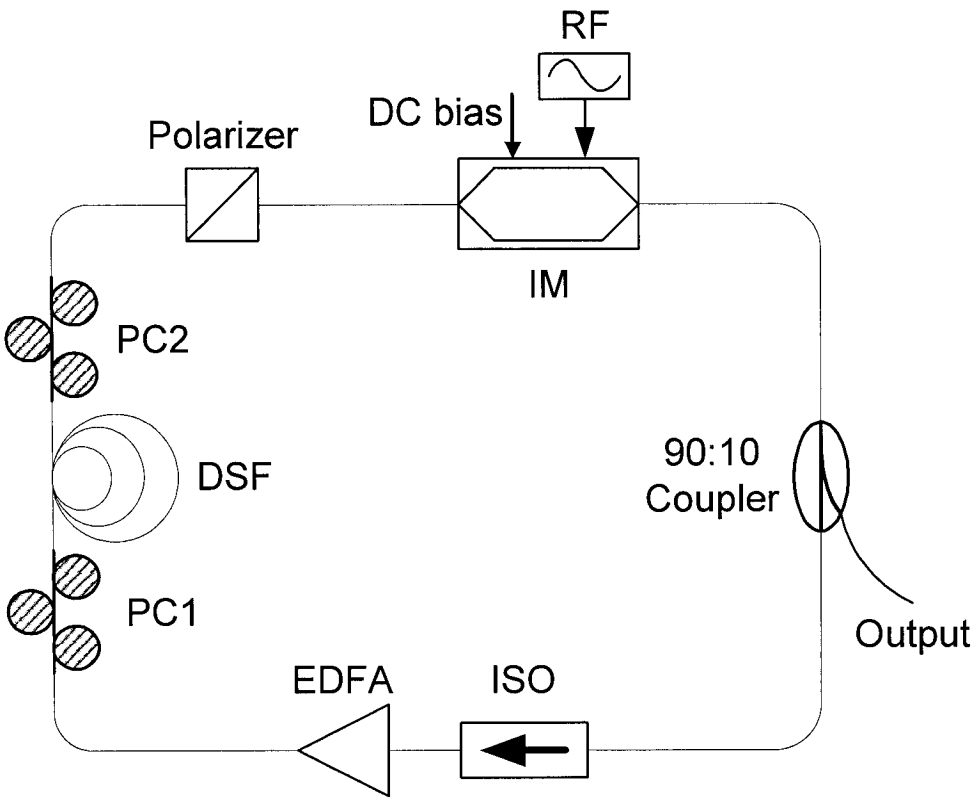

Fig. 5-4. Schematic diagram of the rational harmonic mode-locked ring laser with amplitude equalization by NPR. IM: intensity modulator, ISO: isolator, EDFA: erbium-doped fiber amplifier, PC1, PC2: polarization controllers, DSF: dispersion shifted fiber.

In the following we will briefly discuss the working principle of the NPR pulse amplitude equalizer. One can assume that the NPR effect occurs mainly in the DSF, because of its much smaller effective area than that of the normal single mode fiber. θ_1 is the angle between the polarization direction of the input pulse and the fast axis of the DSF, and θ_2 is the angle between the polarization direction of the output pulse and the polarization direction of the polarizer. Both angles can be controlled by adjusting PC1 and PC2.

It is shown that the transmission of this NPR pulse amplitude equalizer is [Li98]

$$T = \cos^2\theta_1\cos^2\theta_2 + \sin^2\theta_1\sin^2\theta_2 + \frac{1}{2}\sin(2\theta_1)\sin(2\theta_2)\cos(\Delta\phi_L + \Delta\phi_{NL}), \quad (5\text{-}4)$$

where

$$\Delta\phi_L = (n_y - n_x)\beta L, \quad (5\text{-}5)$$

$$\Delta\phi_{NL} = -\frac{n_2 I\beta L}{3}\cos(2\theta_1), \quad (5\text{-}6)$$

n_x and n_y are the linear birefringence coefficients, β is the propagation constant, L is the length of the DSF, n_2 is the nonlinear index coefficient of the DSF, and I is the intensity of the input light.

It is clearly shown in Equation (5-4) that the transmission of the NPR amplitude equalizer depends on the instantaneous power of the light pulse. When θ_1 and θ_2 are set properly, the equalizer acts as a saturable transmitter, whereby a high peak power is suppressed and a low peak power is enhanced. Therefore, pulse amplitude equalization is realized.

The amplitude equalizer utilizing NPR is incorporated into the rational harmonic mode-locked fiber ring laser shown in Fig. 5-1. By tuning the two PCs and the polarizer carefully, we obtain amplitude-equalized pulse train with a repetition rate of 16.5 GHz, which is the third-order harmonic of the modulating frequency. The experiment results are shown in Fig. 5-5, Fig. 5-6, and Fig. 5-7.

Fig. 5-5 shows the beating signals. Although the fundamental and the second-order harmonic frequencies are still visible, they are almost 20 dB lower than the third-order harmonic frequency. Compared to Fig. 5-2, this figure clearly shows the improvement of the NPR type amplitude equalization.

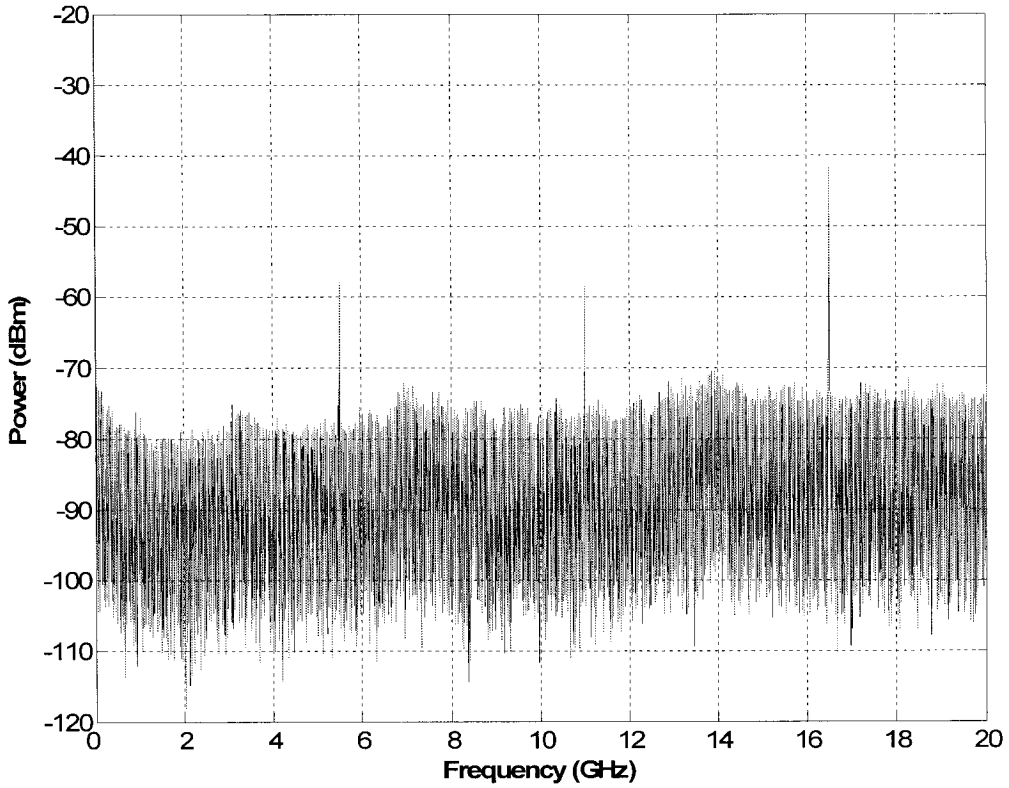

Fig. 5-5. Spectrum of the beating signal of the third-order rational harmonic mode-locked laser with amplitude equalization by NPR.

Fig. 5-6 provides a zoom-in view of the third-order harmonic frequency. It verifies that the linewidth of the generated 16.5 GHz microwave signal is as narrow as 1 Hz. In fact, this measurement is limited by the resolution bandwidth of our spectrum analyzer, which is 1 Hz.

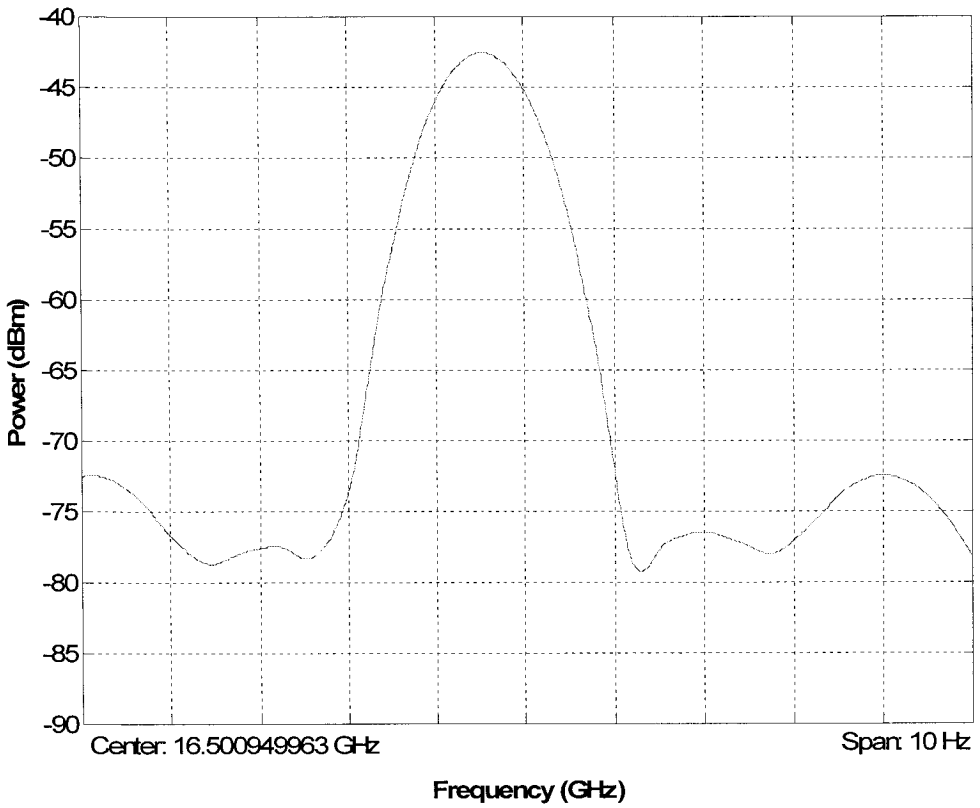

Fig. 5-6. A zoom-in view of the spectrum of the generated microwave signal.

Fig. 5-7 shows the pulse train of the mode-locked laser measured with a high speed oscilloscope. Comparing this figure with Fig. 5-3, which shows the pulse train without amplitude equalization, we can clearly see the improvement brought by the equalizer, although the amplitude flatness is not ideal. This observation agrees with the frequency-domain measurement in Fig. 5-5, which shows that the power of the lower-order harmonic frequencies is reduced. It is believed that further reduction in

the lower-order harmonic power would lead to further improved pulse train amplitude flatness.

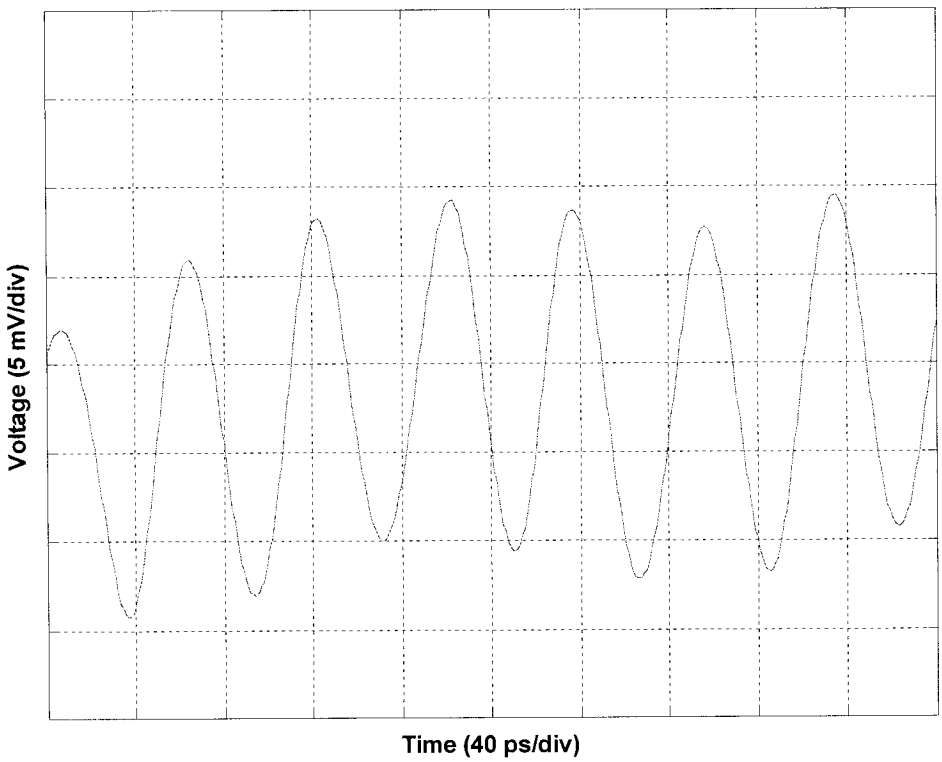

Fig. 5-7. Pulse train of the third-order rational harmonic mode-locked laser with amplitude equalization by NPR.

The proposed rational harmonic mode locked fiber laser can be used to generate high-frequency high-quality microwave signals. However, some drawbacks will limit the application of the fiber laser for microwave generation:

- The structure is too complicate. Very careful adjustment of the PCs and the polarizer is required to get a satisfactory result. For higher-order harmonic generation (more than the fourth-order) this adjustment becomes extremely difficult.
- The equalization of pulse amplitude is not good enough; the lower-order harmonic frequencies are still relatively high.

To simplify the configuration and to further equalize the pulse amplitude, in the following section we will investigate another amplitude equalization technique: nonlinear modulation.

5.4 Amplitude equalization by nonlinear modulation

During the experiment of the rational harmonic actively mode-locked fiber ring laser, we found that the amplitudes of the lower-order harmonic frequencies could be greatly suppressed by adjusting the DC bias voltage of the intensity modulator away

from the linear region. Further experiments proved that when the DC bias point of the intensity modulator was set in the nonlinear region, the amplitude of the pulse train can be equalized without using any extra components. This finding was originally reported in [Fen04].

The analysis of the nonlinear modulation shows [Fen04] that the transfer function of the modulator can be expressed as

$$T(t) = (1-\alpha)\{1-\sin[\pi(b + M\sin(2\pi f_m t))]\}/2, \qquad (5\text{-}7)$$

where α is the insertion loss, b is the normalized bias point of the modulator, M is the normalized amplitude of the modulating signal, or modulation depth, and f_m is the frequency of the modulating signal. This equation indicates that by choosing a different set of b and M, the transfer function of the modulator can have different complex shape during one modulation cycle. If for a certain integer of p, a suitable set of b and M is chosen so that there are p points in a modulation cycle that have the same value of transmission, then the amplitudes of these p pulses must be the same. Thus the amplitude of the p^{th} order harmonic pulses are equalized by the nonlinear modulation.

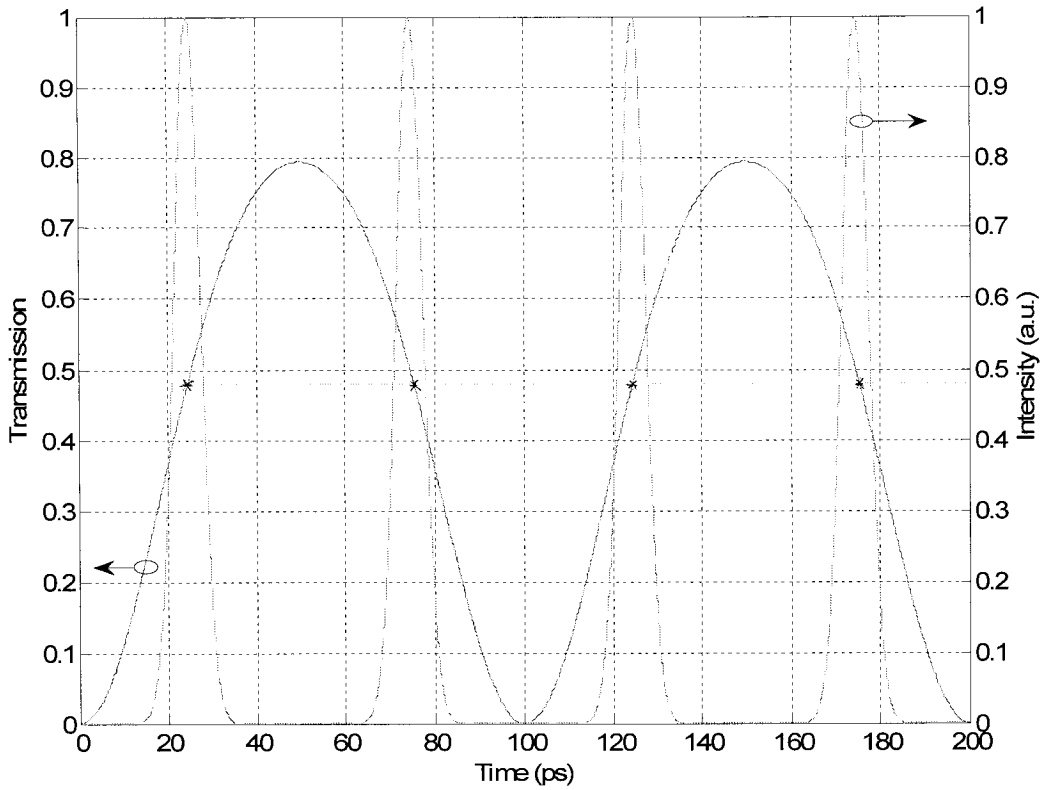

Fig. 5-8. Simulated transfer function of the modulator and the intensity of the pulse train for the 4th order rational harmonic mode locking.

Fig. 5-8 shows the simulation results according to equation (6). The solid line is the transfer function of the modulator when $b=0.5$, $M=0.7$, and $f_m = 5GHz$. The four stars indicate the four points with the same transmission on the transfer function curve. When the optical pulses pass the modulator at the time marked by these four points, the amplitude equalization for the 4th order rational harmonic mode-locking is

therefore realized. The dash line shows the simulated intensity of the optical pulse train under this situation.

With this idea, an experiment on amplitude equalization by nonlinear modulation is implemented. The schematic diagram of the rational harmonic mode-locked ring laser with amplitude equalization using nonlinear modulation is shown in Fig. 5-9. As can be seen the configuration is much more simplified than the fiber laser utilizing NPR.

In this experiment, different combinations of DC bias voltage and amplitude of the modulating signal were investigated to see which one can result in the best performance for amplitude equalization. After several trials, it was found that when the DC bias voltage was set at 1.427 V and the power of the modulating signal was 25 dBm, a fourth-order rational harmonic mode-locked laser was obtained, and the performance of amplitude equalization was the best. By measuring the transfer function of the modulator we used, we found that in this situation the DC bias voltage was set at the minimum transfer point of the modulator. Therefore, this situation is corresponding to the case $b=0.5$, $M=0.7$ in Equation (5-7), and the simulation result is shown in Fig. 5-8.

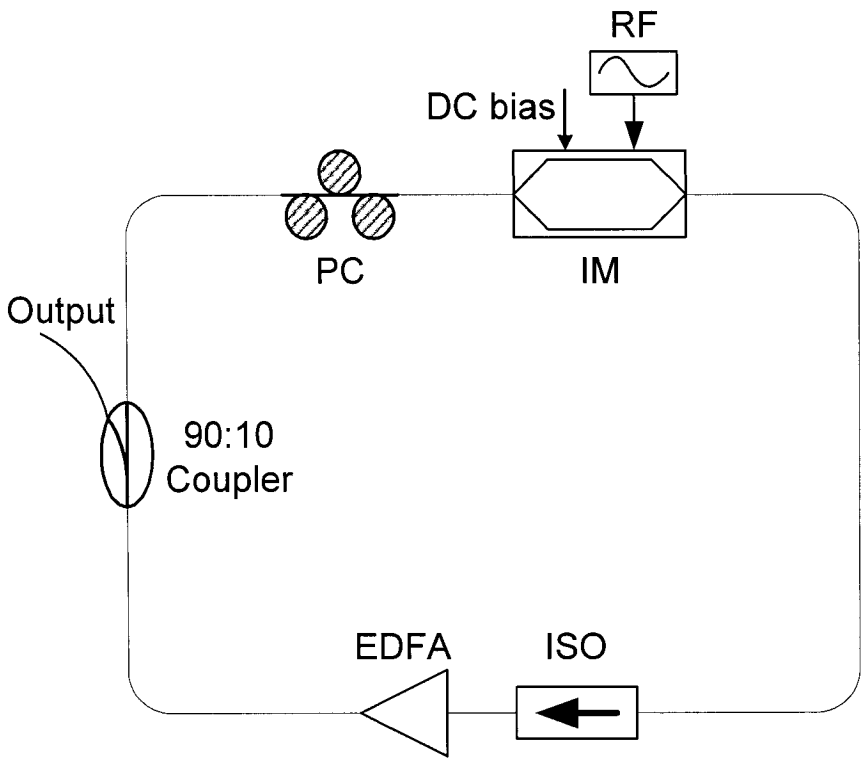

Fig. 5-9. Schematic diagram of the rational harmonic mode-locked ring laser with amplitude equalization by nonlinear modulation. PC: polarization controller, IM: intensity modulator, ISO: isolator, EDFA: erbium-doped fiber amplifier.

The spectrum of the beating signal is shown in Fig. 5-10. As can be seen, a microwave signal at 22 GHz is generated. This frequency is the fourth-order harmonic of the modulating frequency, which is 5.5 GHz. It clearly shows that the fourth-order harmonic frequency is 24 dB stronger than the fundamental and second-order harmonic frequencies. The third-order harmonic is completely suppressed which is below the noise floor. The signal to noise ratio of the generated 22 GHz

signal is 34 dB. This result is obviously much better than the one with the NPR method.

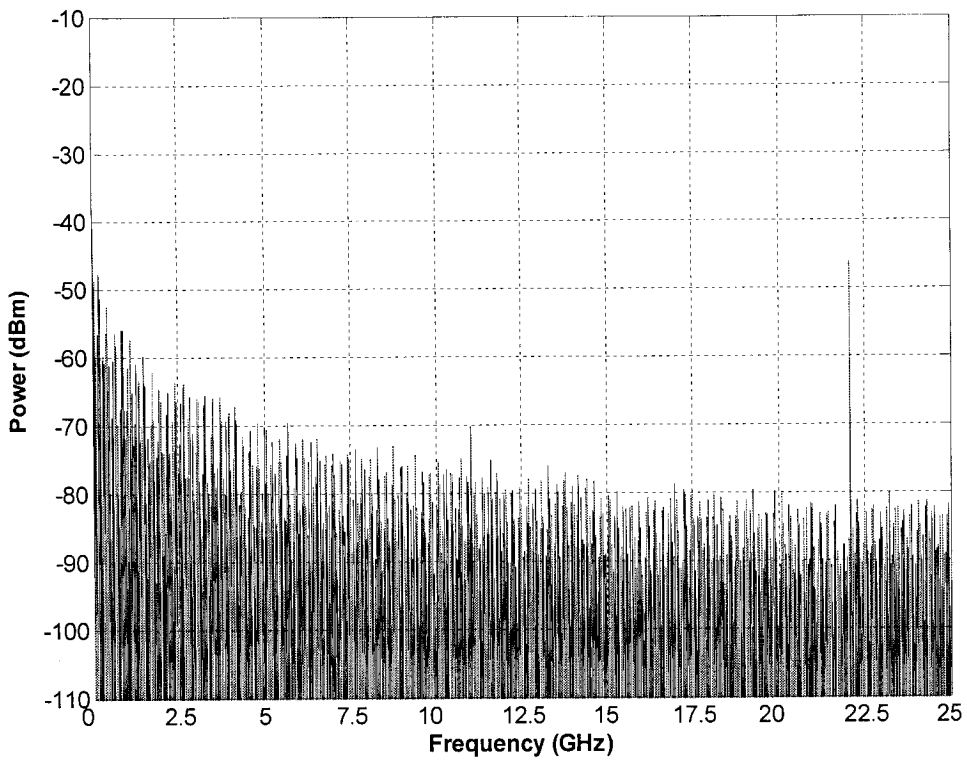

Fig. 5-10. Spectrum of the beating signal generated by the rational harmonic mode-locked laser with amplitude equalization by nonlinear modulation.

Fig. 5-11 shows the zoom-in view of the spectrum of the generated microwave signal. As can be seen that the line-width reaches the smallest resolution bandwidth of the spectrum analyzer, which is 1 Hz. We believe that the actual linewidth would be

smaller. The results reveal that the use of rational harmonic mode locked fiber laser can generate high frequency microwave signal with extremely low phase noise.

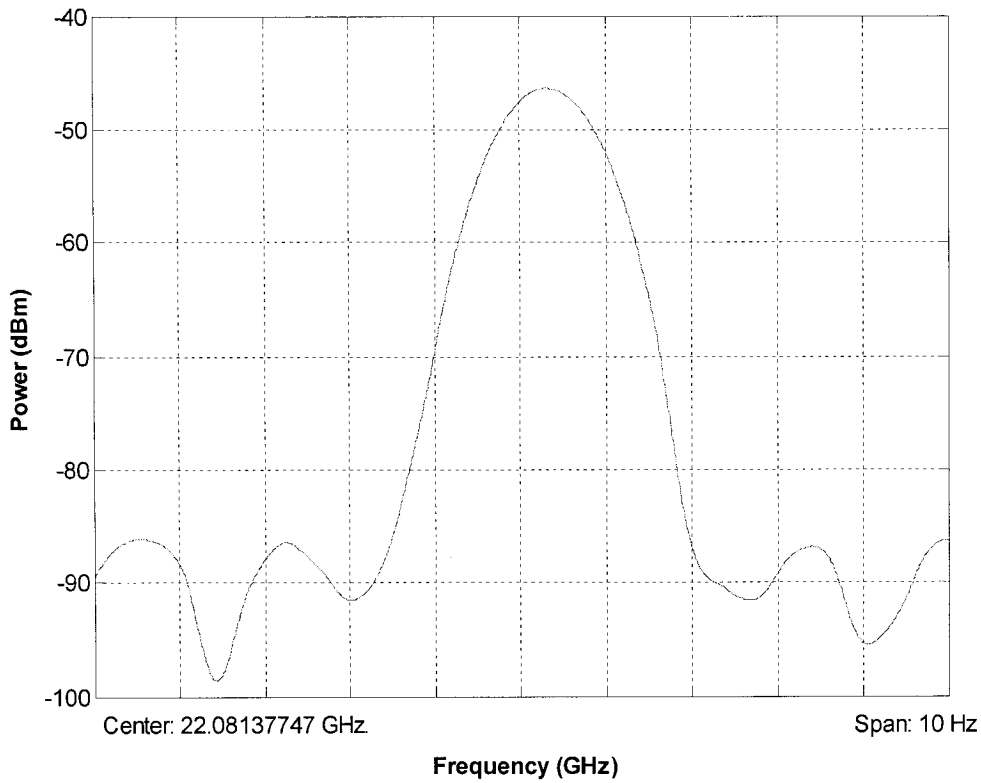

Fig. 5-11. A zoom-in view of the spectrum of the generated microwave signal.

Fig. 5-12 shows the pulse train of the rational harmonic mode-locked laser. Compared to Fig. 5-7, we can see that the amplitude equalization by nonlinear modulation is much better than that by NPR. The pulse amplitude is almost as even as

that of the conventional harmonic mode-locked laser after being equalized by nonlinear modulation.

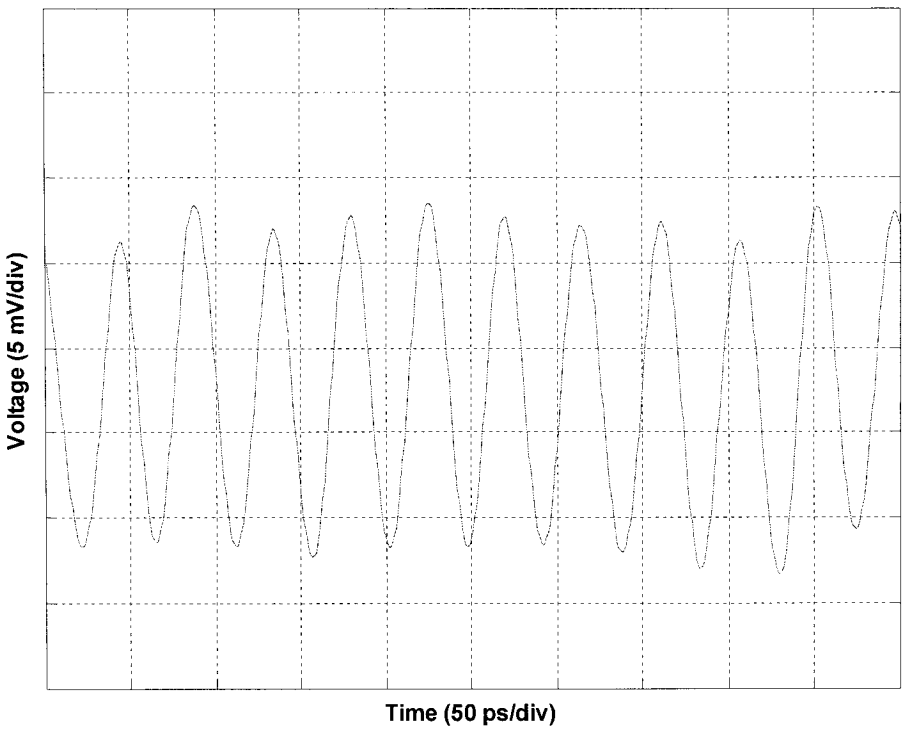

Fig. 5-12. Pulse train of the fourth-order rational harmonic mode-locked laser with amplitude equalization by nonlinear modulation.

5.5 Summary

Rational harmonic actively mode-locked fiber ring lasers and their applications in microwave generation were investigated in this chapter. It was demonstrated that microwave signals generated by a rational harmonic actively mode-locked fiber ring laser can have higher frequencies. To suppress the amplitudes of low-order harmonics, two amplitude equalization techniques were investigated. It was shown that the technique using nonlinear modulation was better than that using NPR. A microwave signal at 22 GHz which was four times the frequency of the modulating signal was generated. Low-frequency components were efficiently suppressed. The generated microwave signal was measured to have a linewidth as narrow as 1 Hz.

Chapter 6 Conclusions and future work

6.1 Conclusions

In this thesis, an investigation was conducted on mode-locked fiber ring lasers and their applications.

In chapter 3, a passively mode-locked fiber ring laser was implemented. A nonlinear amplifying loop mirror (NALM) with an EDFA is used as the mode-locker. With this NALM, a figure-eight laser (F8L) was built. Stable passive mode-locking was achieved. Beating signal with high spectrum quality was obtained by applying the output to a photodetector. The results show that passively mode-locked fiber ring lasers could be used to generate high-quality microwave signals.

In chapter 4, a multiwavelength passively mode-locked fiber ring laser was demonstrated. Three cascaded fiber Bragg gratings (FBGs) were incorporated into the F8L to get three-wavelength lasing. It was different from active mode locking of a multiwavelength fiber laser in which the cavity length for all wavelengths must be

identical. It was demonstrated theoretically and experimentally in this chapter that passive mode locking could be established even if the cavity lengths for different wavelengths were not identical.

In chapter 5, a rational harmonic actively mode-locked fiber ring laser was investigated and demonstrated. A stable microwave signal with frequencies up to 22 GHz was generated by applying the laser output to a photodetector. Rational harmonic mode-locking was better than normal harmonic mode-locking since its repetition rate can be several times higher than the modulating frequency. Thus, it could generate optical pulses with higher repetition rate. One major limitation of the rational harmonic mode locking was that the output pulses have severely uneven amplitudes. To reduce this nonuniformity, nonlinear polarization rotation and nonlinear modulation techniques were utilized to equalize the amplitude in this thesis.

6.2 Future work

1. To achieve passive mode locking a nonlinear device should be used in the laser cavity. In the thesis, NALM using a length of DSF and an EDFA was investigated. Recently, a new type of NOLM named dispersion imbalanced NOLM (DI-NOLM) has been proposed [Seo02]. It has two unique advantages

over the conventional NALMs. First, there are no active components inside the loop. Second, CW light entering the loop mirror will be reflected completely. Therefore, it is expected that the use of the DI-NOLM would increase the performance of passively mode locked fiber lasers.

2. Amplitude equalization is of considerable importance for rational harmonic mode-locked lasers. To improve the stability of the lasers, and to further suppress the unwanted harmonic frequencies, new techniques would be investigated.

3. The stability of a fiber laser is poorer compared to a semiconductor laser, because of the long cavity length of a fiber laser. The problem is expected to be solved if the laser can be implemented using photonic integrated circuits, which may be based on the Silica-on-Silicon integrated optics technology with hybrid active devices or based on III-V Compound Semiconductor photonic integrated circuit technology. For the latter, the material system is InGaAsP quantum well epilayers on InP substrate, and the waveguides are ridge waveguides. With the use of selective area bandgap techniques, including regrowth, selective area growth or selective area multiple-bandgap quantum well intermixing, it is possible to create sections in the photonic integrated circuit with different bandgaps. As such, it permits different sections of the photonic integrated circuit to possess the appropriate bandgaps, such that with respect to the operating wavelength, these

sections would function properly either as passive waveguides, or as laser gain section, saturable absorber, Bragg reflector, photodetector. There is no need for polarization control as the waveguides are highly birefringent. The chief advantage of implementation using a photonic integrated circuit is a very significant reduction of size, as the overall length and width is in a few mm order of magnitude.

REFERENCES

[Agr01] Agrawal, G. P., *Nonlinear Fiber Optics*, 3rd ed., Academic Press, San Diego, CA, 2001.

[Ahm96] Ahmed, Z. and Onodera, N., "High repetition rate optical pulse generation by frequency multiplication in actively modelocked fibre ring lasers," *Electron. Lett.*, vol. 32, no. 5, pp. 455-457, Feb. 1996.

[Bak99] Bakhshi, B. and Andrekson, P. A., "Dual-wavelength 10 GHz actively mode-locked erbium fiber laser," *IEEE Photon. Technol. Lett.*, vol. 11, no. 11, pp. 1387-1389, Nov. 1999.

[Ber92] Bertsekas, D. and Gallager, R., *Data Networks*, 2nd edition, Prentice-Hall, Englewood Cliffs, NJ, 1992.

[Bor99] Bordonaalli, C., Walton, C., and Seeds, A. J., "High-performance phase locking of wide linewidth semiconductor lasers by combined use of optical injection locking and optical phase-lock loop," *J. Lightwave Technol.*, vol. 17, no. 2, pp. 328-342, Feb. 1999.

[Bul90] Bulushev, A. G., Dianov, E. M., and Okhotnikov, O. G., "Passive mode locking of a laser with a nonlinear fiber reflector," *Opt. Lett.*, vol. 15, no. 17, pp. 968-970, Sep. 1990.

[Dor88] Doran, N. J. and Wood, D., "Nonlinear-optical loop mirror", *Opt. Lett.*, vol. 13, no. 1, pp. 56-58, Jan. 1988.

[Dul91] Duling III, I. N., "All-fiber ring soliton laser mode locked with a nonlinear mirror", *Opt. Lett.*, vol. 16, no. 8, pp. 539-541, Apr. 1991.

[Dut98] Dutton, H. J. R., *Understanding optical communications*, International technical Support Organization, 1998.

[Erd97] Erdogan, T., "Fiber grating spectra," *J. Lightwave Technol.*, vol. 15, no. 8, pp. 1277-1294, Aug. 1997.

[Fen04] Feng, X., Liu, Y., Yuan, S., Kai, G., Zhang, W., and Dong, X., "Pulse-amplitude equalization n a rational harmonic mode-locked fiber laser using nonlinear modulation," *IEEE Photon. Technol. Lett.*, vol. 16, no. 8, pp. 1813-1815, Aug. 2004.

[Fer90] Fermann, M. E., Haberl, F., Hofer, M., and Hochreiter, H., "Nonlinear amplifying loop mirror," *Opt. Lett.*, vol. 15, no. 13, pp. 752-754, July 1990.

[Gol83] Goldberg, L., Taylor, H. F., Weller, J. F., and Bloom, D. M., "Microwave signal generation with injection locked laser diodes," *Electron. Lett.*, vol. 19, no. 13, pp. 491-493, June 1983.

[Gol85] Goldberg, L., Yurek, A., Taylor, H. F., and Weller, J. F., "35 GHz microwave signal generation with injection locked laser diode," *Electron Lett.*, vol. 21, no. 18, pp. 814-815, Aug. 1985.

[Har89] Harrison, J. and Mooradian, A., "Linewidth and offset frequency locking of external cavity GaAlAs Lasers," *IEEE J. Quantum Electron.*, vol. 25, no. 6, pp. 1152-1155, June 1989.

[Has95] Hasegawa, A. and Kodama, Y., *Solitons in Optical Communications*, Oxford University Press, New York, NY, 1995.

[Hau75] Haus, H. A., "Theory of mode locking with a fast saturable absorber," *J. Appl. Phys.*, vol. 46, no. 7, pp. 3049-3058, July 1975.

[Hil78] Hill, K. O., Fujii, Y., Johnson, D. C., and Kawasaki, B. S., "Photosensitivity in optical fiber waveguides: Application to reflection filter fabrication," *Appl. Phys. Lett.*, vol. 32, no. 10, pp. 647-649, May 1978.

[Iiz02] Iizuka, K., *Elements of photonics*, John Wiley & Sons, New York, NY, 2002.

[Koe64] Koester, C. J. and Snitzer, E., "Amplification in a fiber laser," *Appl. Opt.*, vol. 3, no. 10, pp. 1182-1186, Oct. 1964.

[Lai01] Lai, Y. C., Zhang, W., and Williams, J. A. R., "Optical generation of tunable microwave signal from a dual mode fiber grating DFB laser," in *2001 International Topical Meeting Microwave Photonics*, pp. 101-103, 2001.

[Lai02] Lai, Y. C., Zhang, W., and Williams, J. A. R., "High frequency signal generation for fibre-radio applications based on a novel fiber laser

structure," *IEEE 7th High Frequency Postgraduate Student Colloquium*, pp. 8-16, Sep. 2002.

[Li98] Li, Y., Lou, C., Wu, J., Wu, B., and Gao, Y., "Novel method to simultaneously compress pulses and suppress supermode noise in actively mode-locked fiber ring laser," *IEEE Photon. Technol. Lett.*, vol. 10, no. 9, pp. 1250-1252, Sep. 1998.

[Li99] Li, S. and Chan, K. T, "A novel configuration for multiwavelength actively mode-locked fiber laser using cascaded fiber Bragg gratings," *IEEE Photon. Technol. Lett.*, vol. 11, no. 2, pp. 179-181, Feb. 1999.

[Li01] Li, Z., Lou, C., Chan, K. T., Li, Y., and Gao, Y., "Theoretical and experimental study of pulse-amplitude-equalization in a rational harmonic mode-locked fiber ring laser," *IEEE J. Quantum Electron.*, vol. 37, no. 1, pp. 33-37, Jan. 2001.

[Lou02] Lou, J. W., Carruthers, T. F., and Currie, M., "Mode-locked multiple-wavelength erbium-doped fiber laser in a Sigma configuration," *IEEE Photon. Technol. Lett.*, vol. 14, no. 3, pp. 281-283, Mar. 2002.

[Mea87] Mears, R. J., Reekie, L., Jauncey, I. M., and Payne, D. N., "Low noise erbium-doped fiber amplifier operating at 1.54 μm," *Electron. Lett.*, vol. 23, no. 19, pp. 1026-1028, Sep. 1987.

[Moo91] Moores, J. D., Bergman, K., Haus, H. A., and Ippen, E. P., "Optical switching using fiber ring reflector," *J. Opt. Soc. Am. B*, vol. 8, no. 3, pp. 594-601, Mar. 1991.

[Mor88] Mortimore, D. B., "Fiber loop reflectors," *J. Lightwave Technol.*, vol. 6, no. 7, pp. 1217-1224, July 1988.

[Nos94] Noske, D. U., Guy, M. J., Rottwitt, K., Kashyap, R., and Taylor, J. R., "Dual-wavelength operation of a passively mode-locked "figure-of-eight" ytterbium-erbium fibre soliton laser," *Opt. Commun.*, vol. 108, pp. 297-301, June 1994.

[Oka00] Okamoto, K., *Fundamentals of optical waveguides*, Academic Press, San Diego, CA, 2000.

[Okh00] Okhotnikov, O. G. and Guina, M., "Stable single- and dual-wavelength fiber laser mode locked and spectrum shaped by a Fabey-Perot saturable absorber," *Opt. Lett.*, vol. 25, no. 22, pp. 1624-1626, Nov. 2000.

[Ono93] Onodera, N., Lowery, A. J., Zhai, L., Ahmed, Z., and Tucker, R. S., "Frequency multiplication in actively mode-locked semiconductor lasers," *Appl. Phys. Lett.*, vol. 62, no. 12, pp. 1329-1331, Mar. 1993.

[Ric90] Richardson, D. J., Laming, R. I., and Payne, D. N., "Very low threshold Sagnac switch incorporating an erbium doped fibre amplifier," *Electron. Lett.*, vol. 26, no. 11, pp. 1779-1781, Oct. 1990.

[Ric91a] Richardson, D. J., Laming, R. I., Payne, D. N., Matsas, V., and Phillips, M. W., "Selfstarting, passively modelocked erbium fibre ring laser based on the amplifying Sagnac switch," *Electron. Lett.*, vol. 27, no. 6, pp. 542-544, Mar. 1991.

[Ric91b] Richardson, D. J., Laming, R. I., Payne, D. N., Phillips, M. W., and Matsas, V. J., "320 fs soliton generation with passively mode-locked erbium fiber laser," *Electron. Lett.*, vol. 27, no. 9, pp. 730-732, Apr. 1991.

[Seo02] Seong, N. H. and Kim, D. Y., "A new figure-eight fiber laser based on a dispersion-imbalanced nonlinear optical loop mirror with lumped dispersive elements," *IEEE Photon. Technol. Lett.*, vol. 14, no. 4, pp. 459-461, Apr. 2002.

[She02] Shen, P., Davies, P. A., Shillue, W. P., D'Addario, L., and Payne, J. M., "Millimeter wave generation using an optical comb generator with optical phase-locked loops," in *international topic meeting on Microwave Photonics, T2-3*, pp. 101-104, 2002.

[Sni61] Snitzer, E., "Optical master action of Nd^{+3} in a barium Crown glass," *Phys. Rev. Lett.*, vol. 7, no. 12, pp. 444-446, Dec. 1961.

[Sot02] Sotobayashi, H., Chujo, W., and Kitayama, K., "1.6-b/s/Hz 6.4-Tb/s QPSK-OCDM/WDM (4 OCDM × 40 WDM × 40 Gb/s) transmission experiment using optical hard thresholding," *IEEE Photon. Technol. Lett.*, vol. 14, no. 4, pp. 555-557, Apr. 2002.

[Sut96] Sutherland, R. L., *Handbook of nonlinear optics*, Marcel Dekker, Inc., New York, NY, 1996.

[Tan03] Tang, W. and Shu, C., "Optical generation of amplitude-equalized pulses from a rational harmonic mode-locked fiber laser incorporating an SOA loop modulator," *IEEE Photon. Technol. Lett.*, vol. 15, no. 1, pp. 21-23, Jan. 2003.

[Tow00] Town, G. E., Chen, L., and Smith, P. W. E., "Dual wavelength modelocked fiber laser," *IEEE Photon. Technol. Lett.*, vol. 12, no. 11, pp. 1459-1461, Nov. 2000.

[Tri88] Trillo, S., Wabnitz, S., Wright, E. M., and Stegeman, G. I., "Soliton switching in fiber nonlinear directional couplers," *Opt. Lett.*, vol. 13, no. 8, pp. 672-674, Aug. 1988.

[Wil89] Williams, K. J., "6-34 GHz offset phase locking of Nd: YAG 1319 nm nonplanar ring lasers," *Electron. Lett.*, vol. 25, no. 18, pp. 1242-1243, Aug. 1989.

[Wu93] Wu, S., Strait, J., Fork, R. L., and Morse, T. F., "High-power passively mode-locked Re-doped fiber laser with a nonlinear optical loop mirror," *Opt. Lett.*, vol. 18, no. 17, pp. 1444-1446, Sep. 1993.

[Yao01] Yao, J., Yao, J. P., Wang, Y., Tjin, S. C., Zhou, Y., Lam, Y. L., Liu, J., and Lu, C., "Active mode locking of tunable multiwavelength fiber ring laser," *Opt. Commun.*, vol. 191, pp. 341-345, May 2001.

[Yos96] Yoshida, E. and Nakazawa, M., "80-200 GHz erbium doped fiber laser using a rational harmonic mode-locking technique," *Electron. Lett.*, vol. 32, no. 15, pp. 1370-1372, July 1996.

[Zak72] Zakharov, V. E. and Shabat, A. B., "Exact theory of two-dimensional self-focusing and one-dimensional self-modulation of waves in nonlinear media (Differential equation solution for plane self focusing and one dimensional self modulation of waves interacting in nonlinear media)," *Sov. Phys. JETP*, vol. 34, pp. 62-69, 1972.

[Zha98] Zhao, Y. and Shu, C., "A fiber laser for effective generation of tunable single- and dual-wavelength mode-locked optical pulses," *Appl. Phys. Lett.*, vol. 72, no. 13, pp. 1556-1558, Mar. 1998.

[Zha01] Zhao, D. and Chan, K. T., "Amplitude equalization of high-repetition-rate pulses in a rational harmonic mode-locked erbium-doped fiber laser with a Fabry-Perot semiconductor modulator," in *Proc. 27th Eur. Conf. on Opt. Comm. (ECOC'01)*, pp. 422-423, 2001.